© 2014. Published by The Company of Biologists Ltd | Development (2014) 141, 2657-2668 doi:10.1242/dev.107573

RESEARCH ARTICLE

The microRNA *bantam* regulates a developmental transition in epithelial cells that restricts sensory dendrite growth

Nan Jiang[1], Peter Soba[2], Edward Parker[3], Charles C. Kim[4] and Jay Z. Parrish[1,*]

ABSTRACT

As animals grow, many early born structures grow by cell expansion rather than cell addition; thus growth of distinct structures must be coordinated to maintain proportionality. This phenomenon is particularly widespread in the nervous system, with dendrite arbors of many neurons expanding in concert with their substrate to sustain connectivity and maintain receptive field coverage as animals grow. After rapidly growing to establish body wall coverage, dendrites of *Drosophila* class IV dendrite arborization (C4da) neurons grow synchronously with their substrate, the body wall epithelium, providing a system to study how proportionality is maintained during animal growth. Here, we show that the microRNA *bantam* (*ban*) ensures coordinated growth of C4da dendrites and the epithelium through regulation of epithelial endoreplication, a modified cell cycle that entails genome amplification without cell division. In *Drosophila* larvae, epithelial endoreplication leads to progressive changes in dendrite-extracellular matrix (ECM) and dendrite-epithelium contacts, coupling dendrite/substrate expansion and restricting dendrite growth beyond established boundaries. Moreover, changes in epithelial expression of cell adhesion molecules, including the beta-integrin *myospheroid* (*mys*), accompany this developmental transition. Finally, endoreplication and the accompanying changes in epithelial *mys* expression are required to constrain late-stage dendrite growth and structural plasticity. Hence, modulating epithelium-ECM attachment probably influences substrate permissivity for dendrite growth and contributes to the dendrite-substrate coupling that ensures proportional expansion of the two cell types.

KEY WORDS: Dendrite, Endoreplication, Extracellular matrix, Growth control, Plasticity, *Drosophila*

INTRODUCTION

A central question in growth control of multicellular organisms is how growing organisms maintain proportionality. This problem is particularly complex when different types of interacting cells must grow in a coordinated fashion, a scenario that is widespread in the nervous system. For example, as animals grow, dendrite arbors of many neurons expand proportionally to sustain proper connectivity and maintain receptive field coverage (Bentley and Toroian-Raymond, 1981; Bloomfield and Hitchcock, 1991; Hitchcock, 1987; Parrish et al., 2009; Truman and Reiss, 1988). This scalar expansion of dendrite arbors to accommodate growth is widely documented in sensory systems, including many types of invertebrate sensory neurons and vertebrate retinal ganglion cells (RGCs). In many cases, dendrites outpace substrate growth to establish appropriate coverage, and subsequently scale with substrate expansion to maintain coverage. Thus, neurons and their substrates differentially respond to common growth cues, receive distinct growth cues, or some combination of both.

Several observations suggest that neuron non-autonomous growth-inhibitory signals contribute to the fidelity of dendrite arbor expansion by restricting dendrite arbors to target fields. Following ablation of RGCs or starburst amacrine cells, the surviving cells developed regularly spaced dendrite arbors that exhibited a limited ability to expand into unoccupied territory (Farajian et al., 2004; Lin et al., 2004). Therefore, interactions between neighboring dendrites are largely dispensable for maintenance of coverage in these neurons and unknown constraints limit their growth potential. Supporting the argument in favor of an extrinsic component, these dendrite arbors expand in sync with retinal growth, whereas exuberant growth is limited.

Drosophila peripheral nervous system (PNS) class IV dendrite arborization (C4da) neurons completely and non-redundantly cover (‘tile’) the larval epidermis early in development and maintain this tiling by growing in precise synchrony with their substrate, the body wall epithelium (Emoto et al., 2006; Grueber et al., 2002; Parrish et al., 2007, 2009). Before establishment of tiling, ablating C4da neurons leads to dendrite growth into vacated territory by adjacent neurons (Grueber et al., 2003; Parrish et al., 2009; Sugimura et al., 2003). However, after tiling is established the invasive growth potential is lost; growth occurs only to maintain proportional receptive field coverage, showing that, as with RGCs, signals constrain late-stage growth of these dendrites. Notably, this signaling does not involve the homotypic repulsion required to establish tiling. Instead, epithelium-derived signals restrict exuberant arbor expansion; the miRNA *ban* acts in epithelial cells to regulate substrate-derived growth-inhibitory signals that constrain dendrite growth (Parrish et al., 2009).

Here, we report our characterization of the *ban*-regulated epithelial signaling that regulates dendrite growth. We found that *ban* regulates epithelial endoreplication, which is required for postembryonic body wall epithelial growth, and that manipulating epithelial endoreplication using *ban*-independent approaches recapitulates *ban*-mediated effects on dendrite growth. Endoreplication influences epithelium-dendrite and epithelium-extracellular matrix (ECM) interactions, providing the cellular basis for the reduced dendrite growth potential that accompanies larval development. At a molecular level, endoreplication alters epithelial expression of cell adhesion molecules, including the integrin Mys, which is required for proper coupling of dendrite and substrate expansion and to restrict dendritic structural plasticity. Thus, a developmental transition in epithelial growth constrains dendrite growth to ensure synchronous expansion of dendrites and their substrate.

[1]Department of Biology, University of Washington, Seattle, WA 98195, USA. [2]Center for Molecular Neurobiology, Hamburg D-20251, Germany. [3]Department of Ophthalmology, University of Washington, School of Medicine, Seattle, WA 98195, USA. [4]Division of Experimental Medicine, Department of Medicine, University of California San Francisco, San Francisco, CA 94110, USA.

*Author for correspondence (jzp2@uw.edu)

Received 26 December 2013; Accepted 6 May 2014

Development (2014) 141, 2657-2668 doi:10.1242/dev.107573

RESULTS

Identification of *ban*-regulated pathways

The microRNA *ban* functions as a regulatory switch for substrate-derived signaling that restricts PNS dendrite growth/plasticity and ensures proportional expansion of dendrite and substrate (Fig. 1A) (Parrish et al., 2009). To identify the substrate-derived factors required for proportional dendrite/substrate growth, we conducted microarray-based expression profiling of epithelial cells from wild-type and *ban* mutant larvae (Fig. 1B). We identified ~100 transcripts that were significantly deregulated in *ban* mutant epithelial cells (Fig. 1C; supplementary material Table S1). Lexical analysis (Kim and Falkow, 2003) indicated that genes associated with the cell cycle were enriched in this dataset, suggesting that *ban* regulates the cell cycle in epithelial cells; we also identified a large number of transcripts associated with cell growth and adhesion.

Drosophila increase their mass ~200-fold during larval development, and this growth is accomplished by cell expansion rather than cell addition (Britton and Edgar, 1998; Church and Robertson, 1966). Indeed, we found that body wall epithelial cell number is constant from late embryogenesis to late larval stages, and that epithelial cells infrequently turn over, as epithelial cell clones persist through larval development >98% of the time (n=200; Fig. 1D,E). Body wall epithelial cell number is unresponsive to *ban* activity (Fig. 1D); thus *ban* regulation of epithelial growth must involve growth of existing cells rather than proliferation. Although *ban* is known to regulate proliferation, and hence growth, in mitotically active tissues (Brennecke et al., 2003; Hipfner et al., 2002), how *ban* regulates growth of differentiated cells is unknown.

To facilitate growth, many larval cell types undergo endoreplication, a modified cell cycle that entails DNA replication without cell division (Britton and Edgar, 1998; Smith and Orr-Weaver, 1991). Consistent with a change in endoreplication, *ban* mutant epithelial cells exhibited dysregulation of cell-cycle-associated genes, including reduced expression of two regulators of endoreplication, *double parked* (*dup*) and *retina aberrant in pattern* (*rap*) (Park and Asano, 2008; Pimentel and Venkatesh, 2005; Sigrist and Lehner, 1997; Zielke et al., 2008), which encode orthologs of the DNA replication factor CDT1 and the APC/C activator CDH1/FZR1, respectively (Fig. 1C). We therefore hypothesized that *ban* regulates growth of mitotic (e.g. imaginal discs) and postmitotic body wall epithelial cells by regulating different forms of the cell cycle.

To monitor larval endoreplication during the period of *ban* activity required for dendrite growth, we fed first instar larvae BrdU for 1 day and monitored BrdU incorporation in third instar larvae. As a positive control we monitored BrdU incorporation in the ventral ganglion, which contains mitotically active neuroblasts and endoreplicating glia (Truman and Bate, 1988; Unhavaithaya and Orr-Weaver, 2012), and observed extensive labeling (Fig. 2A,B). Likewise, we observed extensive labeling of epithelia and muscle, but no labeling of sensory neurons, even when BrdU was constantly administered (Fig. 2C). We therefore conclude that larval body wall epithelia and muscle, but not sensory neurons, endoreplicate.

To monitor the timing and extent of endoreplication in the larval epidermis we measured DNA content in epithelial cells over development. During embryogenesis, epithelial cells and PNS neurons had comparable levels of DAPI staining, and hence DNA content (Fig. 2D,E). Similar to other larval tissues (Britton and Edgar, 1998), body wall epithelia exhibited low levels of endoreplication in first instar larvae; DNA content in epithelial cells was 2.8-fold higher than in PNS neurons. Epithelial ploidy increased throughout larval development, and the rate of endoreplication increased dramatically at 48 h after egg laying (AEL), leading to a ~25-fold increase in genome content by 96 h AEL. Epithelial cell size and ploidy increased at

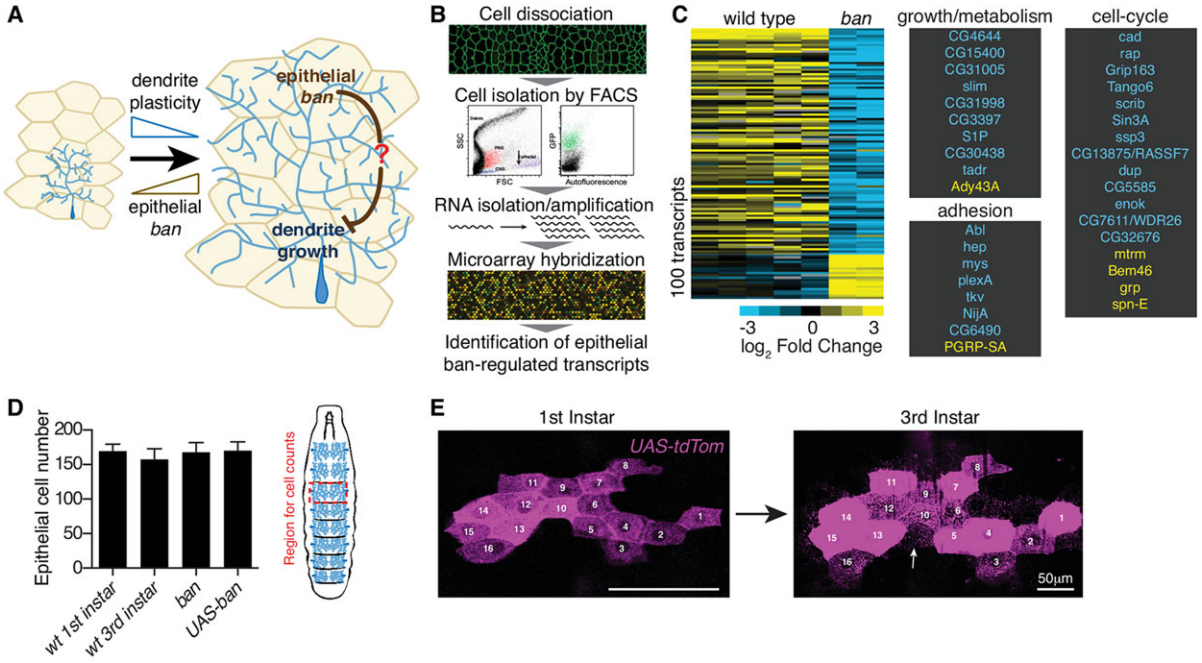

Fig. 1. Identification of substrate-derived regulators of dendrite growth. (A) Schematic depicting the role that *ban* plays in regulating dendrite structural plasticity. (B) Workflow for microarray expression profiling. (C) Heat map depicting *ban*-regulated epithelial transcripts. Transcripts involved in cell growth/metabolism, adhesion, and the cell cycle are listed. (D) Body wall epithelial cell number counts in a region bounded on the anterior and posterior ends by segment borders and on the left and right by C4da neuron cell bodies (hatched rectangle) using DAPI to label nuclei and anti-Mys staining to demarcate cell boundaries. Counts were restricted to segments A2-A4; n≥10 segments for each genotype. (E) Time-lapse imaging of epithelial cell clones in first instar (left) and third instar larvae (right). In this example, all of the cells labeled in first instar (numbered) are present in the same relative position in third instar larvae. Occasionally, additional cells are weakly labeled in third instar larvae (arrow); these cells were present in first instar but tdTomato was undetectable.

Development (2014) 141, 2657-2668 doi:10.1242/dev.107573

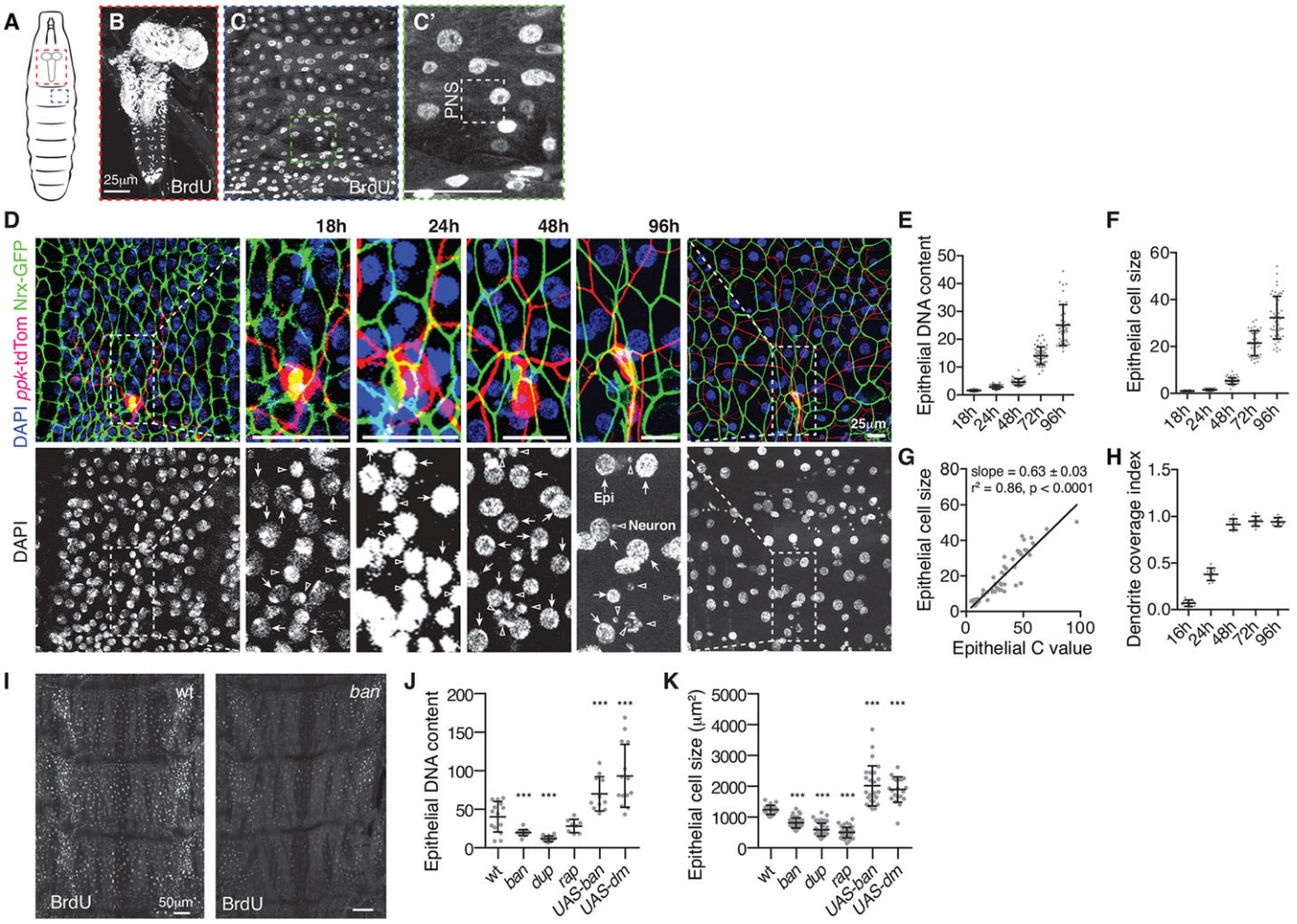

Fig. 2. *ban* regulates a developmental growth transition in epithelial cells. (A-C) BrdU incorporation in *Drosophila* larvae (A), the larval brain (B), and a single dorsal abdominal hemisegment of the larval body wall (C). (C′) Region containing dorsal PNS neurons; these neurons do not incorporate BrdU. (D) Embryos (18 h) or larvae carrying *ppk-tdTomato* (C4da dendrites) and *Nrx-IV::GFP* (epithelia) were injected with DAPI and imaged at the indicated time to allow simultaneous measurement of DNA content, cell size and dendrite coverage. Arrows, epithelial nuclei; carats, neuronal nuclei. (E) Scatter plot, epithelial cell size normalized to the mean epithelial size at 18 h AEL. (F) Scatter plot, epithelial DNA content over development. $n \geq 50$ cells for each time point in E and F. (G) Regression analysis of the relationship between epithelial cell size and DNA content. Ten measurements each from 18 h, 24 h, 36 h, 48 h, 72 h, and 96 h were used for the analysis. The pattern of residuals supports a linear model. (H) Scatter plot depicting dendrite coverage index, the proportion of the body wall covered by C4da dendrites ($n \geq 8$ dendrites at each time point). (I) BrdU incorporation in wild-type (wt) and *ban* mutant larvae. Wild-type and *ban* larvae were processed in the same tube and imaged under identical conditions. (J,K) Scatter plots depict effects of endoreplication on (J) DNA content and (K) cell size in 120 h AEL larvae of the indicated genotype. For J,K, larva were filleted, fixed, and stained with DAPI and Mys antibodies; $n \geq 20$ cells for each genotype. Error bars depict the mean and 95% confidence interval; each data point represents a single cell. *$P<0.05$, **$P<0.01$, ***$P<0.001$, ns, not significant, compared to wild type; one-way ANOVA with a post-hoc Dunnett's test. Scale bars: 25 μm for B-D, 50 μm for H. wt, wild type.

comparable rates, with the pace of epithelial growth dramatically increasing after 48 h AEL (Fig. 2F). Indeed, we observed a strong linear relationship between epithelial DNA content and cell size, suggesting that the two are tightly coupled (Fig. 2G). By contrast, C4da dendrites expanded most rapidly before 48 h AEL, when dendrites establish coverage of a fixed portion of the body wall (Fig. 2H) (Parrish et al., 2009).

ban is required in epithelial cells to dampen dendrite growth beginning at ~48 h AEL (Parrish et al., 2009), after dendrites tile the body wall and coincident with the rapid increase in epithelial endoreplication. We therefore assayed for *ban* function in endoreplication by monitoring BrdU incorporation in *ban* mutant larvae and found that BrdU incorporation was reduced by an average of 56% in *ban* mutant body wall epithelial cells compared with controls (Fig. 2I). Likewise, epithelial ploidy was significantly reduced in *ban* mutants, as in *dup* mutants and larvae with epithelium-specific expression of *dup*(*RNAi*) (Fig. 2J; supplementary material Figs S2 and S3); *rap* mutants exhibited reduced ploidy, but the change was not significant, perhaps owing to protein perdurance. By contrast, epithelial ploidy was significantly increased by overexpression of *ban* or *diminutive* (*dm*; encodes *Drosophila* Myc), which promotes endoreplication in a variety of *Drosophila* cell types (Pierce et al., 2004). Thus, *ban* is necessary and sufficient to promote endoreplication in larval body wall epithelial cells, and the major wave of endoreplication is initiated in second instar larvae, corresponding to the time when *ban* functions in epithelial cells to coordinate dendrite/epithelial growth (Parrish et al., 2009).

We next investigated effects of *ban* activity and endoreplication on epithelial growth. Previously, we found that *ban* mutant body wall lysates had decreased levels of phosphorylated Akt (p-Akt) (Parrish et al., 2009), which is often associated with cell growth. Likewise,

Development (2014) 141, 2657-2668 doi:10.1242/dev.107573

epithelial p-Akt levels were significantly decreased in *ban* mutant and *dup* mutant larvae, whereas p-Akt levels were significantly increased in epithelial cells overexpressing *ban* or *dm* (supplementary material Fig. S1), consistent with *ban* and endoreplication promoting epithelial growth. Indeed, *ban* mutant larvae exhibited significant decreases in epithelial cell size, as did *dup* or *rap* mutants, whereas *ban* or *dm* overexpression significantly increased cell size (Fig. 2K). Thus, *ban* regulates larval endoreplication, which promotes growth of larval epithelial cells.

Epithelial endoreplication influences dendrite growth

C4da dendrite growth outpaces substrate growth to establish tiling, but growth is altered coincident with onset of epithelial endoreplication, such that dendrite arbors expand synchronously with the epidermis to maintain tiling of the growing body wall (Parrish et al., 2009). C4da dendrites in *ban* mutants tile the body wall properly, but dendrite and substrate growth are not synchronized at the first/second instar transition, hence dendrite growth outpaces substrate growth, causing dendrites to occupy larger territories and more densely populate the body wall. As shown in Fig. 3, C4da dendrites in *ban* mutant larvae exhibit a ~30% increase in the territory they cover (coverage index) and a ~140% increase in dorsal midline occupancy as a result of unchecked late-stage growth.

We hypothesized that local signals, independent of systemic cues that promote larval growth and dendrite expansion, coordinate dendrite/substrate growth and that epithelial endoreplication may be a crucial component of this local substrate-derived control of dendrite growth. We therefore assayed effects of epithelial endoreplication on dendrite growth. First, we monitored effects of reducing endoreplication on dendrite growth. In larvae homozygous for mutations in *dup* or *rap*, which attenuate epithelial endoreplication (Fig. 2J), we observed exuberant late-stage dendrite growth similar to *ban* mutants (Fig. 3C,G). Expression of *dup*(*RNAi*) with an epithelium-specific driver (supplementary material Fig. S2) similarly reduced

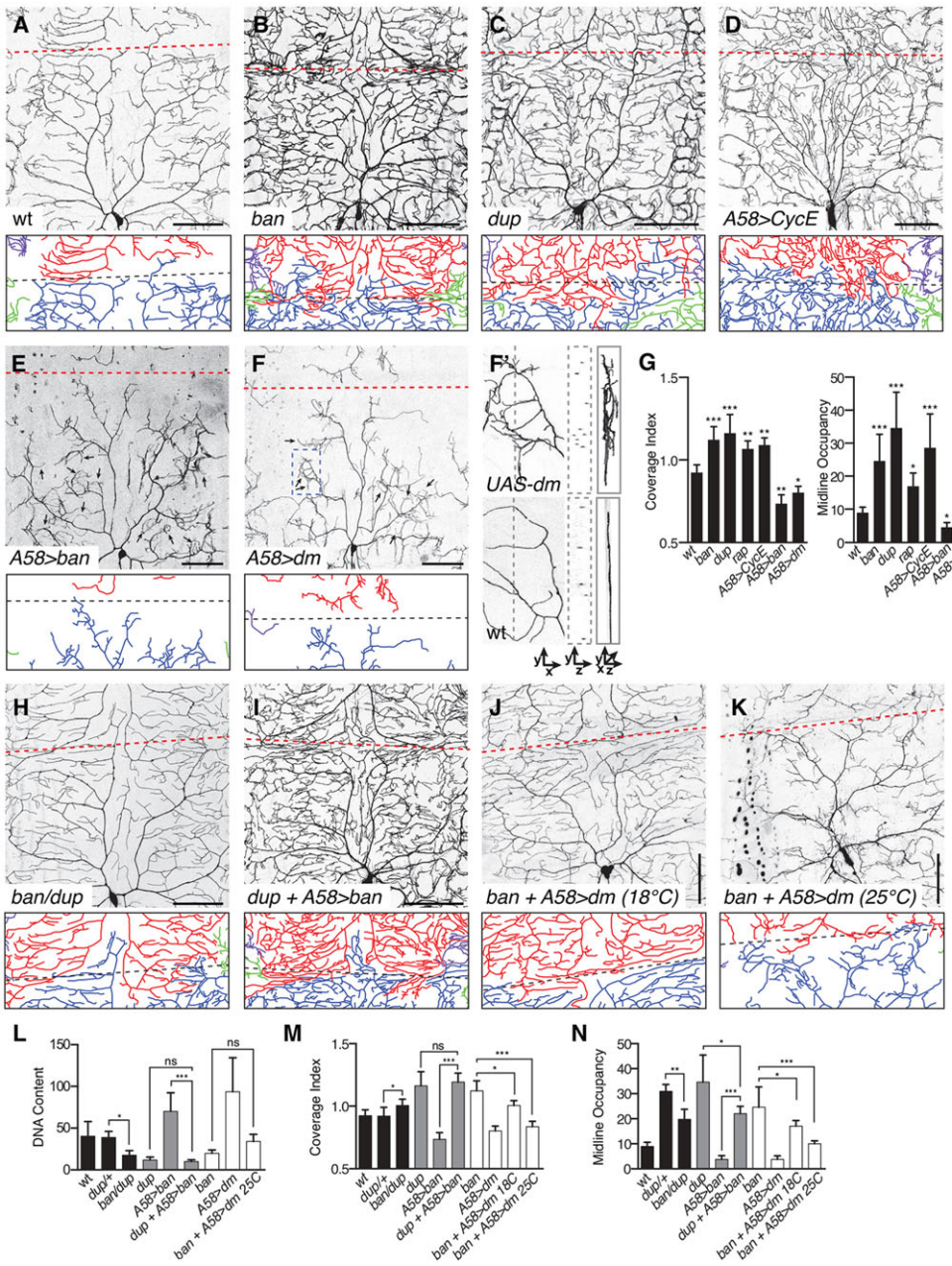

Fig. 3. Epithelial endoreplication influences dendrite growth. (A-D) Effects of reduced epithelial endoreplication on C4da dendrite coverage. Compared to wild type (A), blocking endoreplication with mutations in *ban* (B), *dup* (C), or epithelial *Cyclin E* overexpression (D) increased dendrite growth, including growth beyond normal boundaries (e.g. dorsal midline, hatched line: red in images, black in traces). (E,F) Effects of excess epithelial endoreplication on C4da dendrite growth. Epithelial overexpression of *ban* (E) or *dm* (F) led to reduction in dendrite growth, dendrite wrapping of epithelial cells (arrows) and increased 3D dendrite occupancy. (F′) 3D orientation of dendrites. *yz* cross-section and 3D rendering of region of interest (boxed in F) is shown. A corresponding region is shown for a wild-type C4da dendrite. (G) Quantification of dendrite coverage index and midline occupancy (μm dendrite length/1000 μm^2). (H-N) Epistasis analysis of *ban* and endoreplication machinery. Representative dendrite images of *ban*/*dup* trans-heterozygotes (H), *dup* mutant larvae with epithelial *ban* overexpression (I), and *ban* mutants overexpressing *dm* in epithelial cells reared at 18°C for moderate *dm* expression (J) or 25°C for high *dm* expression (K). Traces depict midline dendrites. $n \geq 8$ neurons for each measurement in G-J. (L-N) Quantification of DNA content, dendrite coverage, and dendrite occupancy from *ban*-endoreplication epistasis analyses. Error bars represent standard deviation. **P*<0.05, ***P*<0.01, ***P*<0.001; ns, not significant; one-way ANOVA with a post-hoc Dunnett's test.

Development (2014) 141, 2657-2668 doi:10.1242/dev.107573

epithelial endoreplication and caused exuberant dendrite growth, whereas resupplying *UAS-dup* to epithelial cells rescued the *dup* mutant dendrite growth defects (supplementary material Fig. S3), demonstrating that *dup* is required in epithelial cells to regulate endoreplication and dendrite growth. Finally, sustained epithelial expression of *Cyclin E*, which inhibits progress through endoreplication cycles (Weiss et al., 1998), caused dendrite defects similar to *ban* mutants (Fig. 3D,G), demonstrating that epithelial endoreplication is necessary for modulation of C4da dendrite growth. By contrast, *ban* or *dm* overexpression, which increases epithelial endoreplication, dampened late-stage dendrite growth, leading to decreased dendrite coverage and midline occupancy (Fig. 3E-G), consistent with a role for epithelial endoreplication in constraining dendrite growth. As with epithelial *ban* overexpression (Parrish et al., 2009), epithelial *dm* overexpression caused dendritic 'wrapping' of epithelial cells, possibly reflecting tighter dendrite-epithelium coupling (Fig. 3F,G). Whereas wild-type C4da dendrites were confined to a thin cross-sectional area along the basal surface of epithelial cells (Fig. 3F′) (Han et al., 2012; Kim et al., 2012), epithelial *dm* or *ban* overexpression caused dendrites to occupy a larger three-dimensional space, particularly in regions exhibiting the 'wrapping' behavior.

To test whether *ban* control of dendrite growth involves epithelial endoreplication, we examined the epistatic relationship between *ban* and endoreplication regulators (Fig. 3H-N). First, we assayed for genetic interactions between *ban* and *dup*. On its own, heterozygosity for mutations in either gene had no significant effect on dendrite coverage or epithelial ploidy, but larvae doubly heterozygous for *ban* and *dup* mutations exhibited modest but significant increases in dendrite coverage and reductions in epithelial ploidy (Fig. 3H,L-N), suggesting that *ban* and the endoreplication effector *dup* function in a genetic pathway to regulate epithelial endoreplication and hence dendrite growth. Second, we overexpressed *ban* in *dup* mutant larvae and found that reducing *dup* function blocked the effects of epithelial *ban* overexpression on dendrite growth and epithelial ploidy (Fig. 3I), demonstrating the requirement for endoreplication in *ban*-mediated dendrite growth control. Third, we overexpressed *dm* in epithelial cells of *ban* mutant larvae, taking advantage of the temperature-sensitive nature of the Gal4-UAS system to drive *dm* expression at different levels. Consistent with *dm* functioning downstream of *ban* to promote endoreplication and constrain dendrite growth, *dm* expression suppressed the dendrite overgrowth and epithelial endoreplication defects of *ban* mutants in a dose-dependent fashion (Fig. 3J,K). Altogether, these results demonstrate that *ban* regulates epithelial endoreplication to modulate dendrite growth.

Developmental control of dendrite-epithelium interactions

Increased epithelial endoreplication alters the relative position of dendrites and epithelial cells (Fig. 3F). We hypothesized that epithelial endoreplication affects dendrite-substrate interactions by promoting epithelium-dendrite adhesion, modulating ECM permissivity to dendrite growth, or some combination of the two. Using a genetically encoded proximity sensor, high-resolution confocal imaging of dendrite/ECM markers, and transmission electron microscopy (TEM) of the dendrite/epithelium interface we examined whether dendrite/epithelium interactions change over developmental time in response to *ban* and endoreplication.

We used GFP reconstitution as a proximity detector (GFP-PD) to monitor dendrite-epithelium apposition with the underlying hypothesis that increased dendrite-epithelium adhesion would be manifest as increased dendrite-epithelium proximity. Based on physical dimensions of the components (Becker et al., 1989; Morell et al., 2008), GFP reconstitution indicates dendrite-substrate proximity of <30 nm, a distance spanned by known adhesion molecules (Fig. 4A). GFP reassembly occurs slowly (Pédelacq et al., 2006); thus dendrite-epithelium apposition must be stable to generate GFP-PD signal. Expressing either half of the proximity sensor produced no GFP-PD signal *in vivo*, whereas neuronal co-expression of both split-GFP fragments resulted in GFP-PD signal throughout the dendritic arbor of first instar larvae (supplementary material Fig. S4), demonstrating that GFP reconstitution occurs on a timescale amenable to analysis of larval dendrite-epithelium proximity.

To monitor dendrite-epithelium juxtaposition we expressed one half of the proximity sensor in C4da neurons and the other half in epithelial cells. In first instar larvae, before the surge in epithelial endoreplication, GFP-PD signal was almost undetectable (Fig. 4B). Epithelial ploidy rapidly increases in second instar larvae, and we likewise observed dendritic accumulation of GFP-PD in second instar larvae (Fig. 4C). Epithelial overexpression of *ban* or *dm* led to a significant increase in GFP-PD in second instar larvae (Fig. 4D,F,G), suggesting that endoreplication promotes dendrite-epithelium juxtaposition. Conversely, *dup* mutants exhibited reduced GFP-PD signal that was most pronounced in terminal dendrites (Fig. 4E-G). We conclude that epithelial endoreplication is necessary and sufficient to trigger developmental changes in dendrite-epithelium juxtaposition.

GFP-PD signal was apparent throughout the majority of the dendritic arbor in third instar larvae (Fig. 4H), suggesting that dendrite-epithelium apposition, and probably adhesion, progressively increases throughout larval development. However, GFP-PD signal was unevenly distributed and markedly reduced/absent from many terminal dendrites, suggesting that dendrite-epithelium apposition varies across the dendritic arbor, with the most dynamic portions (terminal dendrites) coupled to epithelial cells to a lesser degree (Fig. 4H). Epithelial *ban* or *dm* overexpression, by contrast, led to increased levels of GFP-PD signal throughout the dendrite arbor, including terminal dendrites (Fig. 4I), consistent with a role for epithelial endoreplication in promoting dendrite-epithelium adhesion.

C4da dendrites grow along the basal surface of epithelial cells, attached to the ECM by virtue of dendritic integrins, with a small proportion of dendrites embedded in epithelial cells (Han et al., 2012; Kim et al., 2012). Based on our observation that dendritic and epithelial membranes become more closely juxtaposed as larval development progresses, we hypothesized that dendrite-ECM interactions might be developmentally regulated as well. Using high-resolution confocal imaging (Han et al., 2012), we monitored colocalization of dendrites and ECM components labeled by GFP exon traps, including Collagen IV (*vkg-gfp*), and Perlecan (*trol-gfp*) (Fig. 5; supplementary material Figs S5 and S6) (Morin et al., 2001). In first instar larvae, >98% of dendrites co-localize with ECM markers (Fig. 5A,G), but 12% of dendrites in third instar larvae were detached from the ECM and apically shifted (Fig. 5B,G; supplementary material Fig. S5); these detached dendrites are likely embedded in epithelial cells (Han et al., 2012). Significantly fewer dendrites were detached from the ECM in *ban* or *dup* mutant third instar larvae, whereas epithelial *ban* or *dm* overexpression significantly increased apical ECM detachment of dendrites (>25% of dendrites; Fig. 5C-G; supplementary material Fig. S6). Taken together, these results demonstrate that dendrite-epithelium proximity and dendrite-epithelium interactions (embedding) are developmentally regulated by epithelial endoreplication. Thus, after dendritic coverage of the body wall is established, dendrites become increasingly coupled to epithelial cells.

To corroborate our finding that dendrite-epithelium interactions are developmentally regulated by endoreplication, we examined

Development (2014) 141, 2657-2668 doi:10.1242/dev.107573

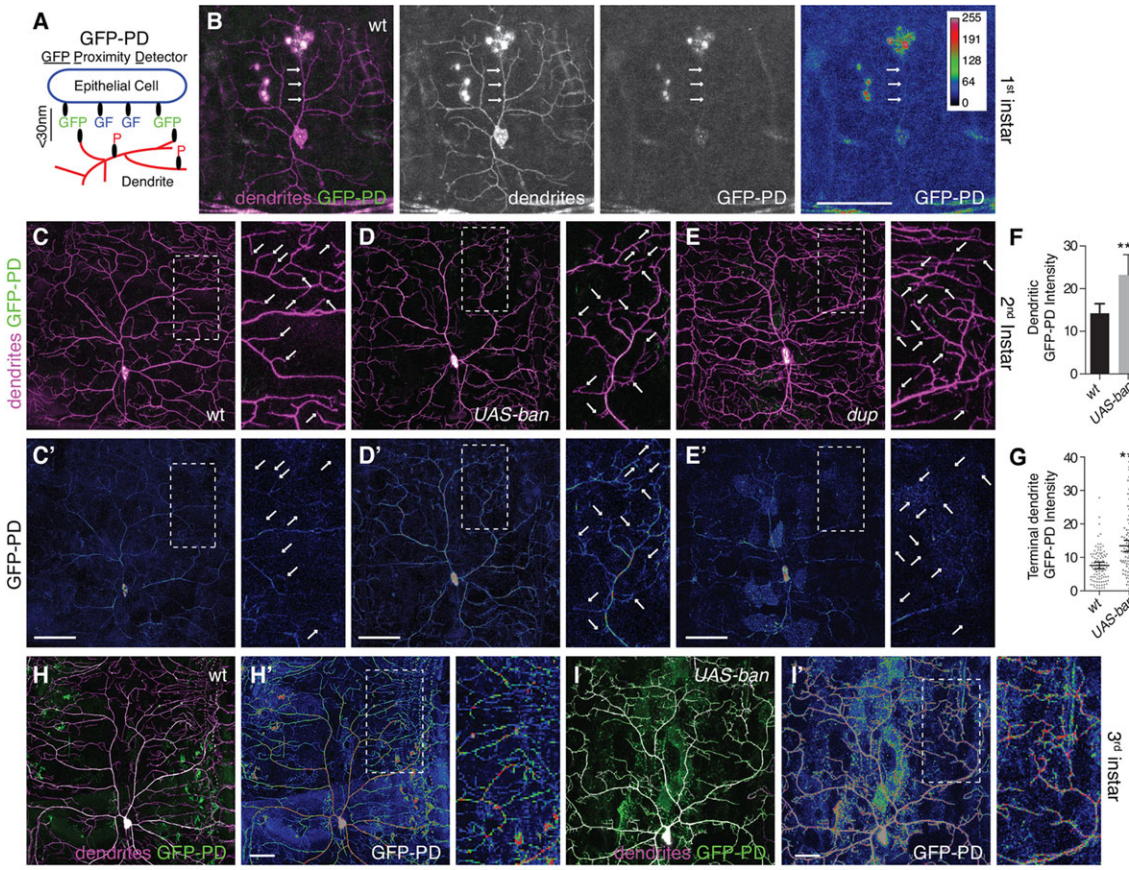

Fig. 4. Dendrite-epithelium proximity is developmentally regulated. (A) GFP-PD schematic. Expressing one membrane-tethered portion of GFP (GF; GFP beta sheet strands 1-10) in epithelial cells and the other membrane-tethered portion in neurons (P; GFP beta sheet strand 11) facilitates high resolution *in vivo* analysis of dendrite-substrate proximity. (B) Dendrite-epithelium GFP-PD signal in first instar larvae. *ppk-spGFP11-CD4-tdTomato* labels dendrites independent of GFP-PD signal. GFP-PD signal is only slightly above background in dendrites (arrows) at this stage; GFP-PD intensity is color-coded according to a lookup table (right). (C-G) Dendrite-epithelia proximity in second instar larvae. *Top*, merged image showing distribution of GFP-PD in the dendrite arbor of wild type (C), epithelial *ban* overexpressing (D) or *dup* mutant (E) larvae. *Bottom*, GFP-PD intensity. Arrows mark tips of a subset of terminal dendrites. (F) Quantification of dendrite-epithelium GFP-PD signal from second instar larvae. Intensity values were measured along the entire dendrite arbor; mean values (following background subtraction) for ten neurons of each genotype are plotted. Error bars, standard deviation. (G) Scatter plot showing the mean and 95% confidence interval for terminal dendrite GFP-PD intensity ($n \geq 200$ terminal dendrites for each genotype). *$P<0.05$, **$P<0.01$, ***$P<0.001$, ns, not significant, compared to wild type; one-way ANOVA with a post-hoc Dunnett's test. (H-I) Dendrite-epithelia GFP-PD signal in third instar larvae. Epithelial *ban* overexpression leads to increased GFP-PD signal intensity, especially in terminal dendrites, suggesting that *ban* promotes dendrite-substrate proximity. Scale bars: 50 μm.

dendrite-epithelium interactions using TEM. In thin sections of abdominal segments cut along the apicobasal body wall axis, we monitored distribution of dendrites (identified as processes near the basal epithelial surface containing arrays of parallel microtubules) and the frequency of plasma membrane invaginations, as internalized dendrites are frequently found in membrane invaginations (Han et al., 2012; Kim et al., 2012). In first instar larvae, most dendrites were positioned at the surface of epithelial cells in direct contact with the ECM; only 3/50 dendrites were enclosed in epithelial cells (Fig. 5H; supplementary material Fig. S7). We observed a substantial increase in epithelium-embedded dendrites in third instar larvae (27/91 dendrites; Fig. 5H). Thus, dendrite-epithelium interactions change substantially from early larval development when dendrites establish body wall coverage to late larval development when dendrites expand proportionally with their substrate. The frequency of membrane invaginations significantly increased in third instar larvae (supplementary material Fig. S7), and this may facilitate dendrite enclosure by epithelial cells. Mutations that inhibited endoreplication blocked the developmental increase in epithelial plasma membrane invagination and dendrite enclosure, whereas treatments that increased epithelial endoreplication had the opposite effects (Fig. 5H; supplementary material Fig. S7). These findings confirm our results using a GFP-based proximity sensor and our *in vivo* imaging of dendrite-ECM colocalization; altogether, these studies indicate that dendrite-epithelium interactions are developmentally regulated and that endoreplication in epithelial cells is a crucial component of this control.

Next, we set out to identify molecular mediators of this developmentally regulated change in dendrite-epithelium interaction. Most *ban*-responsive adhesion-related transcripts were differentially expressed in first and third instar epithelial cells, consistent with *ban* playing a role in developmental control of epithelial adhesion (Fig. 1C and Fig. 6A). We therefore examined whether expression of these adhesion-related genes was responsive to endoreplication. Notable among these transcripts were *mys*, which encodes the lone somatically expressed *Drosophila* β-integrin, and *hep*, which encodes a *Drosophila* JNK kinase; integrins are key mediators of cell-ECM interactions including epidermis-basement membrane attachment (DiPersio et al., 1997), and JNK regulates adhesive properties of *Drosophila* epithelial cells (Jacinto et al., 2000; Jasper et al., 2001; Martin-Blanco et al., 2000). Epithelial Mys levels, in particular on the basal surface of epithelial cells outside of the basolateral junctional domain (Fig. 6B; arrows, adherens junctions), significantly increased

Development (2014) 141, 2657-2668 doi:10.1242/dev.107573

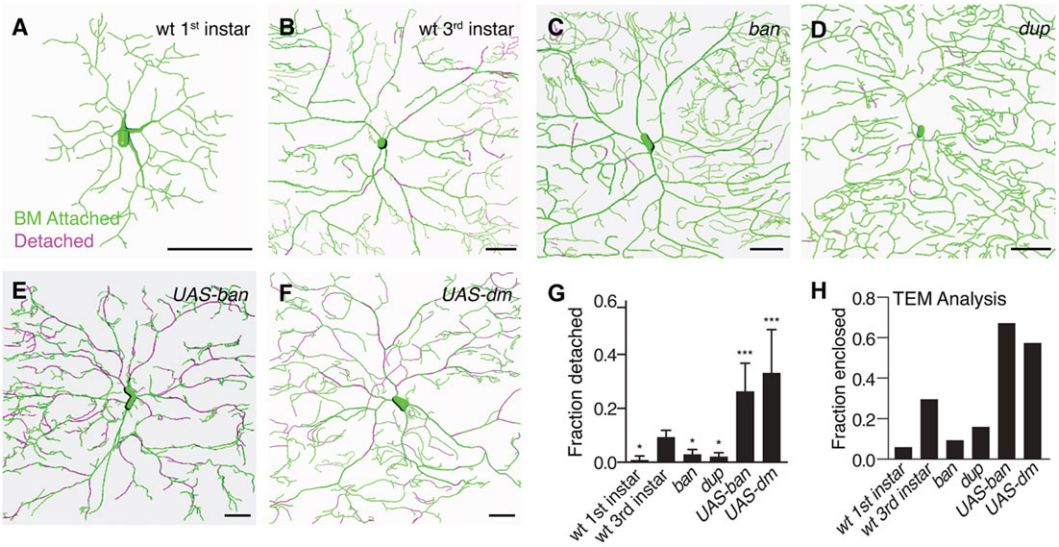

Fig. 5. Epithelial endoreplication influences dendrite-ECM attachment. Live imaging of dendrites and ECM using a neuronal membrane marker (*ppk-CD4-tdTomato*) and a *collagen IV* exon trap (*vkg-GFP*) to monitor dendrite-ECM colocalization in first instar wild-type (A), third instar wild-type (B), *ban* mutant (C), epithelial *ban* overexpressing (D), *dup* mutant (E) and epithelial *dm* overexpressing larvae (F). Representative maximum projections of 3D stacks are shown (A,B). Following deconvolution, colocalization was measured between dendrites and Vkg-GFP (see supplementary material Fig. S5); in traces, green depicts dendrites that colocalize with Vkg-GFP and magenta depicts detached (apically shifted) dendrites. Similar results were obtained using an additional ECM marker (supplementary material Fig. S6). (G) Quantification of dendrite detachment from the ECM ($n \geq 10$ neurons for each genotype). (H) TEM analysis. The fraction of dendrites enclosed inside epithelial cells is shown ($n \geq 50$ dendrites for all genotypes). Other than wild-type first instar samples, all samples were from third instar larvae. *$P<0.05$, **$P<0.01$, ***$P<0.001$ compared to wild-type third instar; one-way ANOVA with a post-hoc Dunnett's test.

during larval development, concomitant with the rapid increase in larval endoreplication, suggesting that Mys expression is coupled to endoreplication. Indeed, Mys expression was dampened by mutations that reduced endoreplication, and epithelial *ban* or *dm* overexpression, which increase endoreplication, further enhanced Mys levels (Fig. 6B). Likewise, phosphorylated JNK (P-Jnk) levels significantly increased during larval development and this increase was dependent on *ban* as well as endoreplication (supplementary material Fig. S8). Thus, developmental changes in epithelial expression of adhesion-related genes are triggered by endoreplication. We therefore hypothesized that endoreplication affects dendrite growth via changes in epithelial adhesion.

Epithelium-ECM interactions influence dendrite growth and plasticity

To examine whether epithelial integrins influence dendrite growth, we expressed *UAS-mys*(*RNAi*) in epithelial cells, which attenuated epithelial Mys protein levels (supplementary material Fig. S9), and monitored effects on dendrite patterning in third instar larvae. Epithelial *mys*(*RNAi*) caused exuberant late-stage dendrite growth similar to *ban* mutants or other endoreplication-defective mutants, albeit to a lesser extent (Fig. 6C,F). Thus, increased expression of Mys, which mediates ECM attachment, contributes to coordination of dendrite/epithelial growth by constraining late-stage dendrite growth. One model to account for this finding is that increased epithelium-ECM attachment makes the ECM less permissive to dendrite growth. Alternatively, increased epithelium-ECM attachment may potentiate epithelium-dendrite contacts that constrain dendrite growth.

To ascertain whether developmental control of Mys expression is a functionally relevant output of *ban* in regulating dendrite growth, we examined the epistatic relationship between epithelial *ban* and *mys* in control of C4da dendrite development. First, we simultaneously overexpressed *ban* and knocked down *mys* in epithelial cells and found that *mys*(*RNAi*) attenuated the dendrite growth defect of *ban* overexpression, resulting in dendrite overextension beyond normal boundaries (Fig. 6D,F). Second, we assayed effects of epithelial overexpression of integrins (*UAS-mys +UAS-inflated*) on dendrite growth and found that integrin overexpression caused a dendrite undergrowth phenotype similar to that of *ban* or *dm* overexpression (Fig. 6E,F). Third, we overexpressed integrins in *ban* mutant larvae and found that epithelial integrin overexpression only partially suppressed the dendrite overgrowth of *ban* mutants (Fig. 6F). We conclude that increased epithelial Mys expression is necessary but not sufficient for *ban*-mediated control of dendrite growth. Taken together with our observation that modulating integrin expression causes less severe dendrite defects than modulation of *ban* or endoreplication, these results suggest that additional epithelium-derived factors contribute to *ban*-mediated, and hence endoreplication-dependent, epithelial control of dendrite growth.

Ablating C4da neurons before establishment of tiling leads to exuberant dendrite growth into unoccupied territory by spared neurons and this invasive growth potential is lost concomitant with the onset of epithelial endoreplication (Grueber et al., 2003; Parrish et al., 2009; Sugimura et al., 2003). We therefore hypothesized that developmental restriction in C4da dendrite plasticity is the result of alterations in dendrite-substrate and dendrite-epithelium interactions triggered by epithelial endoreplication, including increased proximity dendrite-epithelium proximity. Indeed, following ablation of a C4da neuron, invading dendrites of spared neurons were less closely associated with epithelial cells than neighboring non-invading dendrites, as assessed by relative levels of GFP-PD intensity (Fig. 7A-C).

ECM modification plays important roles in regulating dendrite structural plasticity in several contexts (Mataga et al., 2002; Oray et al., 2004; Yasunaga et al., 2010), thus we reasoned that *ban*-regulated changes in epithelium-ECM attachment might alter substrate permissivity for dendrite growth and hence C4da dendrite plasticity. To test this possibility, we ablated second instar Cd4a neurons and monitored dendrite invasion of the unoccupied territory by spared

Development (2014) 141, 2657-2668 doi:10.1242/dev.107573

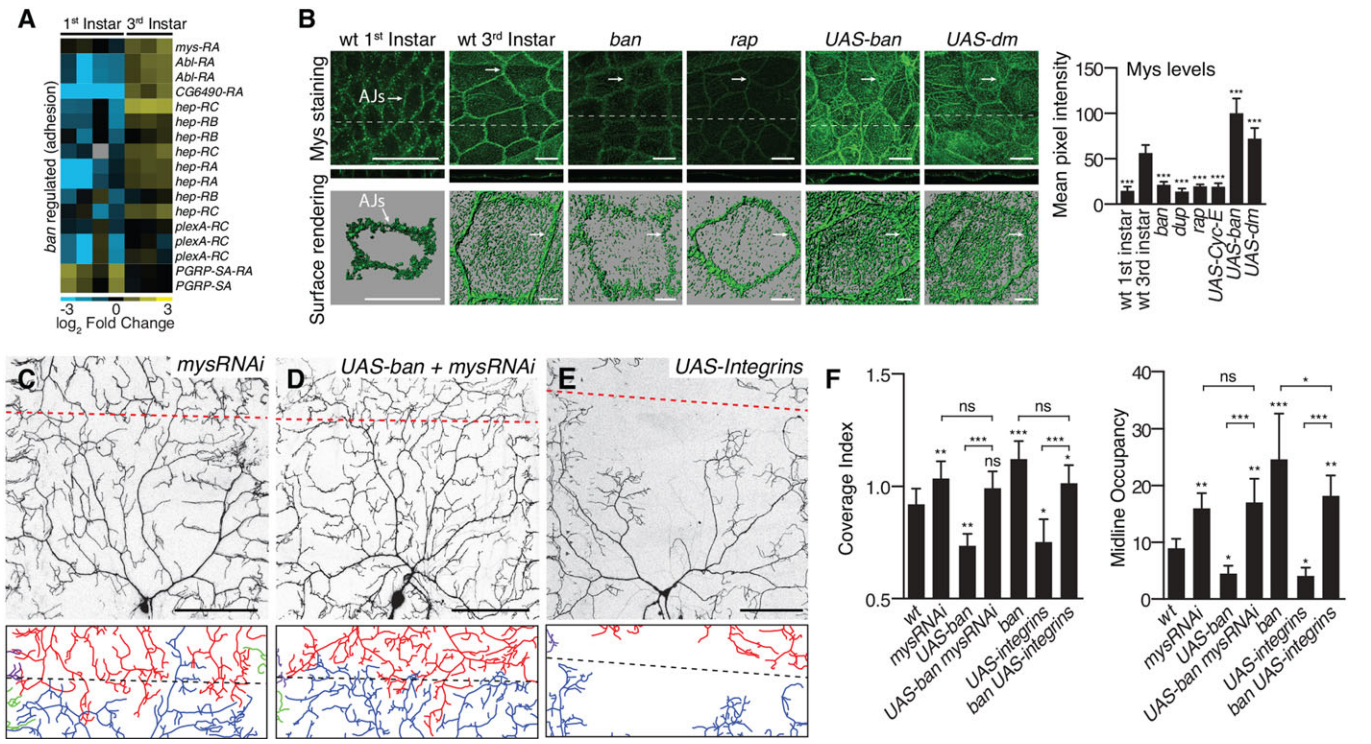

Fig. 6. Developmental changes in epithelial adhesion influence dendrite growth. (A) Heat map depicting developmental expression of *ban*-regulated adhesion molecules in epithelial cells. (B) Developmental regulation of epithelial Mys expression. Top, larval fillets of the indicated genotype stained with Mys antibody. Images are maximum projections of *z*-stacks; dashed lines, position of orthogonal slices. Bottom, 3D rendering of Mys distribution. Right, Quantification of Mys immunoreactivity in the indicated genotypes. $n \geq 50$ cells for each genotype. (C-F) Epithelial integrin influences dendrite growth. Representative C4da dendrites and midline dendrite traces for epithelial *mys*(*RNAi*) (C), epithelial co-expression of *UAS-mys*(*RNAi*) and *UAS-ban* (D), and epithelial expression of *UAS-integrins* (E). (F) Quantification of dendrite coverage index and midline occupancy (μm dendrite length/1000 μm^2). $n \geq 8$ neurons for each measurement. Error bars represent standard deviation. **P*<0.05, ***P*<0.01, ****P*<0.001, ns, not significant; one-way ANOVA with a post-hoc Dunnett's test. Scale bars: 25 μm in B, top; 10 μm in B, bottom; 50 μm in C-E.

neurons. In this paradigm, wild-type dendrites exhibit little invasive activity, covering ~18% of vacated territory (Fig. 7D,G). By contrast, when we ablated C4da neurons in *dup* mutant larvae, which are defective in endoreplication and the associated developmental changes in dendrite-epithelium interactions, we observed robust invasive activity comparable to *ban* mutants (Fig. 7E,G). Likewise, when we reduced epithelial Mys levels via epithelia-specific *mys*(*RNAi*), we observed a significant potentiation of dendrite invasion (Fig. 7F,G). Notably, mutations in *ban* or *dup* potentiate dendrite invasion to a greater degree than *mys*(*RNAi*) (Fig. 7G; Parrish et al., 2009), suggesting that factors other than *mys* function downstream of endoreplication to control dendrite expansion. We conclude that the developmentally programmed growth transition to endoreplication in epithelial cells regulates substrate permissivity for dendrite growth, in part by regulating epithelium-ECM interactions.

DISCUSSION

Local and systemic control of dendrite growth

During embryonic and early larval development, C4da dendrites expand faster than their substrate to achieve complete body wall coverage. C4da neurons respond to nociceptive stimuli (Tracey et al., 2003), and the rapid early dendrite growth ensures that the larval body wall is completely covered by these sensory dendrites shortly after hatching, when larvae must interact with their surroundings. Subsequently, C4da dendrites expand synchronously with the body wall epithelium as larvae grow while maintaining proportionality (Fig. 8A). Thus, multiple growth signals are likely to be at work in this system. In response to systemic growth cues, dendrites and epithelial cells continuously expand during larval development. Blocking these growth cues, for example by ablating dILP neurons or compromising insulin signaling, similarly affects both neuron and substrate, resulting in growth-arrested larvae with properly scaled dendrite arbors (Parrish et al., 2009). Beginning in second instar larvae, sensory neurons and epithelial cells respond differently to growth cues: epithelial growth relies on endoreplication; sensory neuron growth does not (Fig. 8B). During this latter period of larval growth, epithelium-derived signals constrain dendrite expansion to ensure synchronous dendrite/substrate growth. Larval activation of *ban* in epithelial cells is an essential component of this signaling cascade (Parrish et al., 2009), and here we demonstrate that *ban* functions in epithelial cells to regulate endoreplication. By altering adhesive properties of epithelial cells, hence epithelium-ECM and epithelium-dendrite interactions, endoreplication curtails C4da dendrite growth and plasticity (Fig. 8C). Many types of neuron expand their arbors synchronously with their substrate to maintain proportional coverage of their receptive field; developmental control of substrate adhesion may be similarly regulated in other contexts to couple dendrite/substrate growth, and to regulate dendrite structural plasticity.

Endoreplication in nervous system development

Growth control is particularly complex in the nervous system, where different cell types are continuously incorporated and cells must grow while maintaining connections. In some contexts, programmed polyploidy facilitates neuronal growth. For example, in the terrestrial slug *Limax valentianus* endoreplication occurs

Development (2014) 141, 2657-2668 doi:10.1242/dev.107573

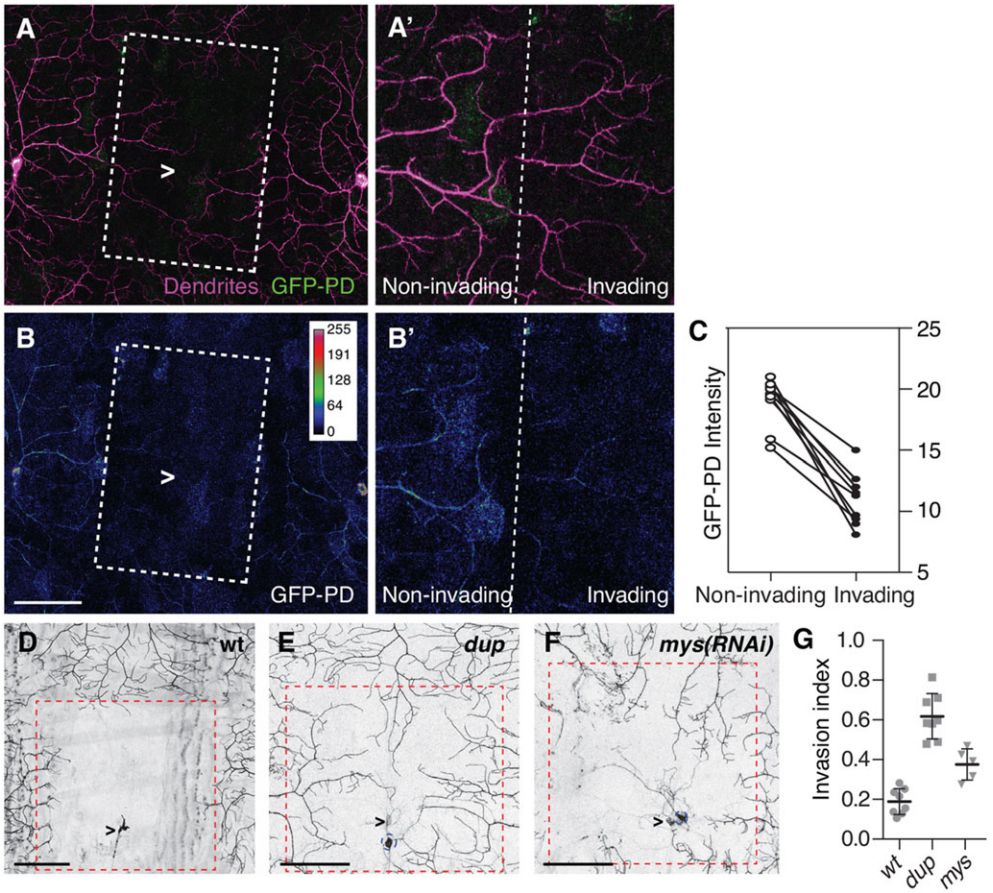

Fig. 7. Epithelium-BM attachment influences dendrite structural plasticity. (A-C) Dendrite-epithelium interactions differ in invading/non-invading dendrites. Merged image (A) and GFP-PD signal (B) 48 h post-ablation (carat, soma; white box, dendritic territory of ablated neuron). (A′,B′) Dendrite growth and GFP-PD signal at the receptive field boundary (dashed line) of the ablated neuron. Invading dendrites grow beyond this boundary and non-invading dendrites remain on the left of side of the boundary. Neurons express *ppk-spGFP11-CD4-tdTomato* and epithelia express *UAS-spGFP1-10-CD4-mCer*. (C) Mean GFP-PD intensity values for invading dendrites and neighboring non-invading dendrites from the same neuron (n=9 neurons). (D-G) Second instar C4da neurons were laser-ablated and dendrite invasion into unoccupied territory was monitored 48 h post-ablation in (D) Control, (E) *dup* mutant and (F) epithelium-specific *mys* (*RNAi*) larvae. Hatched red boxes demarcate territory covered by the ablated neuron and carats mark the position of the ablated cell body. Class III neurons are stochastically labeled (blue dashed circles). (G) Scatter plot depicting mean and standard deviation for dendrite invasion ($n\geq8$ neurons for each genotype).

throughout the nervous system in proportion to animal growth, presumably to facilitate neuron expansion (Yamagishi et al., 2011). Neuronal polyploidy has been documented in vertebrates as well; tetraploid neurons exist in the retina and cortex (López-Sánchez and Frade, 2013; Morillo et al., 2010), and Purkinje neurons may be polyploid (Lapham, 1968; Mann et al., 1978).

In addition to supporting neuronal growth, developmentally regulated polyploidy (endoreplication) is suited for tissue growth in circumstances where division might disrupt patterning or connectivity. For example, endoreplication allows glial cells that wrap the *Drosophila* ventral ganglion to maintain blood-brain barrier integrity even as glia grow to accommodate brain expansion (Unhavaithaya and Orr-Weaver, 2012). Likewise, we found that epithelial endoreplication allows for substrate growth without cell divisions that might disrupt body wall innervation. In addition, epithelial endoreplication drives a differentiation program that regulates epithelium-dendrite interactions to influence sensory dendrite growth and patterning. Notable among these interactions is an increase in epithelial dendrite embedding, which may serve a number of purposes. First, as suggested in prior studies, embedding may have functional consequences (Han et al., 2012; Kim et al., 2012). Second, embedding may provide points of contact that constrain dendrite expansion. Third, embedding may facilitate generation of tensile forces as the body wall expands; such forces could contribute to dendrite growth, analogous to axon elongation in response to mechanical tension (Bray, 1984). How genome amplification potentiates certain signaling pathways is unknown, but *Drosophila* endoreplication entails under-replication of specific genomic regions in a cell-type-specific manner (Sher et al., 2013), thus endoreplication may facilitate expression of an epithelium-differentiation program. It remains to be seen whether endoreplication regulates substrate or target-derived signals that influence neuron growth and patterning in other systems.

Substrate control of dendrite plasticity

Here, we demonstrate that dendrite plasticity is tied to growth control. We found that alterations in substrate adhesive properties constrain dendrite plasticity in C4da neurons concomitant with proportional expansion of dendrites and substrate. First, decreased plasticity is accompanied by increased dendrite-epithelium proximity during development; manipulations that increase plasticity decrease dendrite-epithelium proximity, and vice versa. Second, epithelial dendrite embedding, which may serve to tether dendrites to epithelial cells, increases as the capacity for structural plasticity decreases, and manipulations that increase plasticity decrease the prevalence of epithelium-embedded dendrites. Third, epithelial adhesion changes as dendritic plasticity is restricted and epithelial integrin expression contributes to restriction of plasticity. Large-scale plasticity would seem to be incompatible with synchronous growth of neurons and their substrate, so it will be intriguing to see whether dendritic plasticity is broadly constrained during periods of growth that maintain proportionality.

MATERIALS AND METHODS

Fly stocks

See supplementary material Table S2 for alleles used in this study.

Live imaging

Embryos were collected on yeasted grape juice agar plates, aged at 25°C in a moist chamber, mounted in 90% glycerol under coverslips sealed with

Development (2014) 141, 2657-2668 doi:10.1242/dev.107573

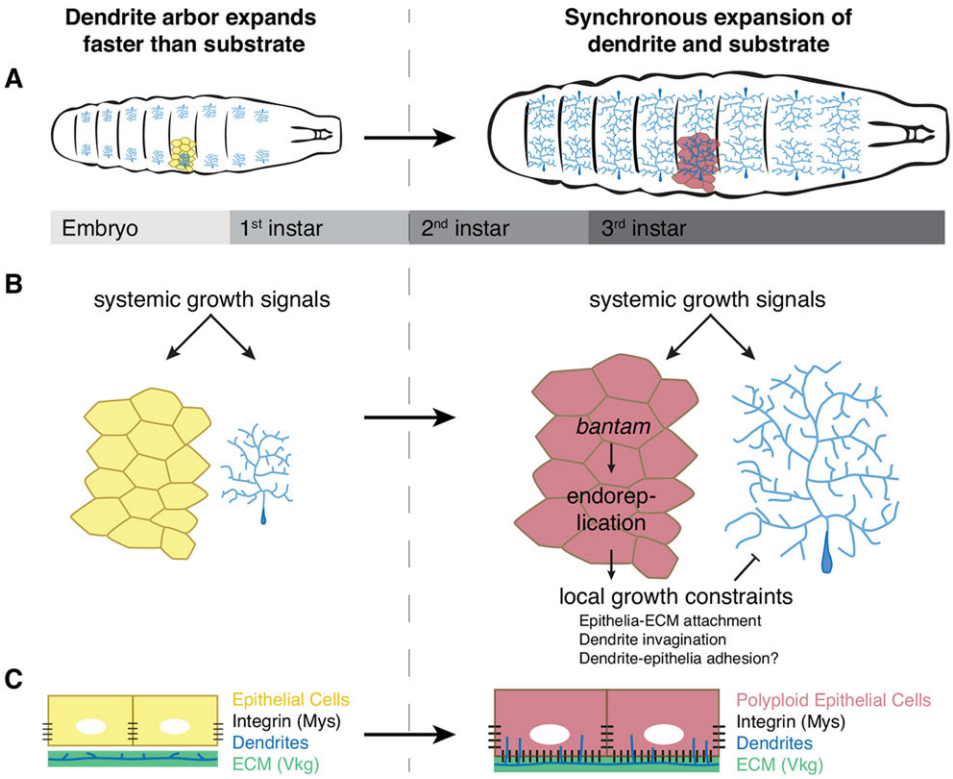

Fig. 8. Biphasic control of larval dendrite expansion. (A) Dendrites outgrow their substrate to establish complete coverage of the epidermis. After the first/second instar transition, dendrites expand in proportion to their substrate. (B) Larval dendrites and epithelial cells constantly grow in response to systemic cues. Epithelial endoreplication alters adhesive properties of epithelial cells, locally constraining dendrite growth. (C) Epithelial expression of β-Integrin (black dashed lines) and epithelial invagination of dendrites (blue) are developmentally regulated.

grease and imaged using a Leica SP5 microscope with a 40×, 1.25NA lens. To analyze dendrite phenotypes, image stacks of dendrites in segments A2-A4 were captured from 8-10 larvae. For high-resolution imaging of the dendrite-ECM interface, larvae were anesthetized with ether before mounting and stacks with a 0.2 µm *z*-step were acquired.

GFP reconstitution

GFP proximity detection (GFP-PD) is based on GRASP constructs (Feinberg et al., 2008) using extracellular GFP fragments tethered to the transmembrane carrier CD4. Briefly, CD4-spGFP1-10 was PCR amplified and cloned into pUAST containing a C-terminal mCerulean tag. Transgenic lines were obtained from BestGene (Chino Hills, CA). *UAS-spGFP1-10-CD4-mCer* was recombined with *ppk-spGFP11-CD4-tdTomato* (Han et al., 2012) and epithelium-dendrite GFP reconstitution was monitored using the epithelium-specific *A58-Gal4* driver to express *UAS-spGFP1-10-CD4-mCer* with the C4da neuron-specific *ppk-spGFP11-CD4-tdTomato*. GFP-PD signal was imaged under identical conditions for all samples of a given time point, taking care to avoid pixel saturation. Dendrite arbors were used to generate a mask, and mean GFP-PD pixel intensity within the mask was measured using ImageJ (NIH).

Laser ablation

A single larva was mounted, as for live imaging, and the nucleus of a C4da neuron was targeted under a 100×-1.4NA objective using a 337 nm pulsed nitrogen laser (Andor Micropoint; 12 Hz, 15 s) mounted on a Leica DM550 microscope. Following ablation, animals were recovered to cornmeal agar and imaged 48 h later.

Immunohistochemistry

Larval immunohistochemistry was as described (Grueber et al., 2002) using the following: HRP-Cy2 or Cy3 (1:200; Jackson ImmunoResearch), mCD8 (1:100; Life Technologies), phospho-D-Akt Ser505 (1:500; Cell Signaling), Myospheroid-CF.6G11 (1:20; Developmental Studies Hybridoma Bank), BrdU (1:250; Abcam), phospho-JNK (1:500; Cell Signaling), DAPI (50 ng/ml; Life Technologies) and secondary antibodies from Jackson ImmunoResearch. For BrdU labeling, larvae were fed cornmeal-molasses food containing BrdU (10 µg/ml; Sigma), dissected in PBS, fixed in 4% formaldehyde/PBS, permeabilized in PBS-Tx, acid treated with 2.5 N HCl for 30 min, neutralized with 100 mM sodium tetraborate, and processed for immunostaining.

TEM

Larvae were perforated with insect pins, fixed in 2.5% glutaraldehyde/0.1 M sodium cacodylate buffer with centrifugation [15,000 rpm (21,330 ***g***), 1 h], washed 4×5 min in PBS and post-fixed at 4°C in buffered 2% osmium tetroxide overnight. Samples were spun [12,500 rpm (14,674 ***g***), 1 h], washed with distilled water in 20 ml scintillation vials (3×20 min), and dehydrated in a graded series of ethanol, followed by two changes of propylene oxide. This was followed by infiltration in a 1:1 mixture of propylene oxide:epon-araldite overnight, two changes in epon-araldite (2 h each), and overnight polymerization (60°C). 70 nm sections were stained with Reynolds' lead citrate and viewed on a JEOL-1230 microscope with an AMT XR80 camera.

Microarray analysis

Fluorescence-activated cell sorting (FACS) cell purification and microarray analysis were conducted as described (Parrish et al., 2014). Details are available in in the supplementary materials and methods.

Measurements

Dendrite metrics: 2D projections of *z*-stacks were used for computer-assisted dendrite tracing (Neurolucida); arbor features were measured using the traces. Details are provided in the supplementary materials and methods.

DNA content: DAPI quantitation was as described (Unhavaithaya and Orr-Weaver, 2012). Briefly, we measured pixel intensity of DAPI stain in each optical section of *z*-stacks (500 nm step) and normalized epithelial DAPI intensity to mean DAPI intensity of ten diploid PNS neurons from the same fillet imaged using identical settings. PNS neuron DAPI intensity varied less than 10%.

Cell size: We traced the outline of Nrx-IV-GFP or anti-Mys immunoreactivity for ≥50 epithelial cells of each genotype using ImageJ (NIH). We obtained similar results with volume measurements of epithelial cells.

Development (2014) 141, 2657-2668 doi:10.1242/dev.107573

Statistical analysis

Differences between group means were analyzed via ANOVA with a post-hoc Dunnett's test. Significance of microarray expression was calculated using Significance analysis of microarrays (SAM) (Tusher et al., 2001) using a 5% false discovery rate and fold-change threshold of 1.5-fold. Lexical analysis was as described (Kim and Falkow, 2003).

Accession number

Microarray data are available in the NCBI Gene Expression Omnibus (GSE50540).

Acknowledgements

We thank the Bloomington Stock Center, Chun Han, Yuh Nung Jan and Paul Lasko for fly stocks; the DSHB for antibodies; the CHDD for assistance with TEM; Hui Li and Jon Ahn for assistance with stereology; and Michael Kim for critical reading of the manuscript.

Competing interests

The authors declare no competing financial interests.

Author contributions

N.J. and J.P. conceived and designed the experiments. N.J. and J.P. conducted the experiments with assistance from P.S. on GFP reconstitution assays, C.K. on microarray analysis, and E.P. on TEM. N.J., C.K. and J.P. analyzed the data. J.P. wrote the manuscript.

Funding

This work was supported by the National Institutes of Health (NIH) [NIMH-R00MH084277 and NINDS-R01NS076614], by a Basil O'Connor Starter Scholar Award, by a Klingenstein Fellowship in Neuroscience (J.Z.P.) and by a Benjamin Hall Graduate Fellowship (N.J.). Deposited in PMC for release after 12 months.

Supplementary material

Supplementary material available online at
http://dev.biologists.org/lookup/suppl/doi:10.1242/dev.107573/-/DC1

References

Becker, J. W., Erickson, H. P., Hoffman, S., Cunningham, B. A. and Edelman, G. M. (1989). Topology of cell adhesion molecules. *Proc. Natl. Acad. Sci. U.S.A.* **86**, 1088-1092.

Bentley, D. and Toroian-Raymond, A. (1981). Embryonic and postembryonic morphogenesis of a grasshopper interneuron. *J. Comp. Neurol.* **201**, 507-518.

Bloomfield, S. A. and Hitchcock, P. F. (1991). Dendritic arbors of large-field ganglion cells show scaled growth during expansion of the goldfish retina: a study of morphometric and electrotonic properties. *J. Neurosci.* **11**, 910-917.

Bray, D. (1984). Axonal growth in response to experimentally applied mechanical tension. *Dev. Biol.* **102**, 379-389.

Brennecke, J., Hipfner, D. R., Stark, A., Russell, R. B. and Cohen, S. M. (2003). bantam encodes a developmentally regulated microRNA that controls cell proliferation and regulates the proapoptotic gene hid in Drosophila. *Cell* **113**, 25-36.

Britton, J. S. and Edgar, B. A. (1998). Environmental control of the cell cycle in Drosophila: nutrition activates mitotic and endoreplicative cells by distinct mechanisms. *Development* **125**, 2149-2158.

Church, R. B. and Robertson, F. W. (1966). Biochemical analysis of genetic differences in the growth of Drosophila. *Genet. Res.* **7**, 383-407.

DiPersio, C. M., Hodivala-Dilke, K. M., Jaenisch, R., Kreidberg, J. A. and Hynes, R. O. (1997). α3β1 Integrin is required for normal development of the epidermal basement membrane. *J. Cell Biol.* **137**, 729-742.

Emoto, K., Parrish, J. Z., Jan, L. Y. and Jan, Y.-N. (2006). The tumour suppressor Hippo acts with the NDR kinases in dendritic tiling and maintenance. *Nature* **443**, 210-213.

Farajian, R., Raven, M. A., Cusato, K. and Reese, B. E. (2004). Cellular positioning and dendritic field size of cholinergic amacrine cells are impervious to early ablation of neighboring cells in the mouse retina. *Vis. Neurosci.* **21**, 13-22.

Feinberg, E. H., Vanhoven, M. K., Bendesky, A., Wang, G., Fetter, R. D., Shen, K. and Bargmann, C. I. (2008). GFP Reconstitution Across Synaptic Partners (GRASP) defines cell contacts and synapses in living nervous systems. *Neuron* **57**, 353-363.

Grueber, W. B., Jan, L. Y. and Jan, Y. N. (2002). Tiling of the Drosophila epidermis by multidendritic sensory neurons. *Development* **129**, 2867-2878.

Grueber, W. B., Ye, B., Moore, A. W., Jan, L. Y. and Jan, Y. N. (2003). Dendrites of distinct classes of Drosophila sensory neurons show different capacities for homotypic repulsion. *Curr. Biol.* **13**, 618-626.

Han, C., Wang, D., Soba, P., Zhu, S., Lin, X., Jan, L. Y. and Jan, Y.-N. (2012). Integrins regulate repulsion-mediated dendritic patterning of drosophila sensory neurons by restricting dendrites in a 2D space. *Neuron* **73**, 64-78.

Hipfner, D. R., Weigmann, K. and Cohen, S. M. (2002). The bantam gene regulates Drosophila growth. *Genetics* **161**, 1527-1537.

Hitchcock, P. F. (1987). Constant dendritic coverage by ganglion cells with growth of the goldfish's retina. *Vis. Res.* **27**, 17-22.

Jacinto, A., Wood, W., Balayo, T., Turmaine, M., Martinez-Arias, A. and Martin, P. (2000). Dynamic actin-based epithelial adhesion and cell matching during Drosophila dorsal closure. *Curr. Biol.* **10**, 1420-1426.

Jasper, H., Benes, V., Schwager, C., Sauer, S., Clauder-Münster, S., Ansorge, W. and Bohmann, D. (2001). The genomic response of the Drosophila embryo to JNK signaling. *Dev. Cell* **1**, 579-586.

Kim, C. C. and Falkow, S. (2003). Significance analysis of lexical bias in microarray data. *BMC Bioinformatics* **4**, 12.

Kim, M. E., Shrestha, B. R., Blazeski, R., Mason, C. A. and Grueber, W. B. (2012). Integrins establish dendrite-substrate relationships that promote dendritic self-avoidance and patterning in drosophila sensory neurons. *Neuron* **73**, 79-91.

Lapham, L. W. (1968). Tetraploid DNA content of Purkinje neurons of human cerebellar cortex. *Science* **159**, 310-312.

Lin, B., Wang, S. W. and Masland, R. H. (2004). Retinal ganglion cell type, size, and spacing can be specified independent of homotypic dendritic contacts. *Neuron* **43**, 475-485.

López-Sánchez, N. and Frade, J. M. (2013). Genetic evidence for p75NTR-dependent tetraploidy in cortical projection neurons from adult mice. *J. Neurosci.* **33**, 7488-7500.

Mann, D. M. A., Yates, P. O. and Barton, C. M. (1978). The DNA content of Purkinje cells in mammals. *J. Comp. Neurol.* **180**, 345-347.

Martin-Blanco, E., Pastor-Pareja, J. C. and Garcia-Bellido, A. (2000). JNK and decapentaplegic signaling control adhesiveness and cytoskeleton dynamics during thorax closure in Drosophila. *Proc. Natl. Acad. Sci. U.S.A.* **97**, 7888-7893.

Mataga, N., Nagai, N. and Hensch, T. K. (2002). Permissive proteolytic activity for visual cortical plasticity. *Proc. Natl. Acad. Sci. U.S.A.* **99**, 7717-7721.

Morell, M., Czihal, P., Hoffmann, R., Otvos, L., Avilés, F. X. and Ventura, S. (2008). Monitoring the interference of protein-protein interactions in vivo by bimolecular fluorescence complementation: the DnaK case. *Proteomics* **8**, 3433-3442.

Morillo, S. M., Escoll, P., de la Hera, A. and Frade, J. M. (2010). Somatic tetraploidy in specific chick retinal ganglion cells induced by nerve growth factor. *Proc. Natl. Acad. Sci. U.S.A.* **107**, 109-114.

Morin, X., Daneman, R., Zavortink, M. and Chia, W. (2001). A protein trap strategy to detect GFP-tagged proteins expressed from their endogenous loci in Drosophila. *Proc. Natl. Acad. Sci. U.S.A.* **98**, 15050-15055.

Oray, S., Majewska, A. and Sur, M. (2004). Dendritic spine dynamics are regulated by monocular deprivation and extracellular matrix degradation. *Neuron* **44**, 1021-1030.

Park, S. Y. and Asano, M. (2008). The origin recognition complex is dispensable for endoreplication in Drosophila. *Proc. Natl. Acad. Sci. U.S.A.* **105**, 12343-12348.

Parrish, J. Z., Emoto, K., Jan, L. Y. and Jan, Y. N. (2007). Polycomb genes interact with the tumor suppressor genes hippo and warts in the maintenance of Drosophila sensory neuron dendrites. *Genes Dev.* **21**, 956-972.

Parrish, J. Z., Xu, P., Kim, C. C., Jan, L. Y. and Jan, Y. N. (2009). The microRNA bantam functions in epithelial cells to regulate scaling growth of dendrite arbors in drosophila sensory neurons. *Neuron* **63**, 788-802.

Parrish, J. Z., Kim, C. C., Tang, L., Bergquist, S., Wang, T., DeRisi, J. L., Jan, Y. N., Jan, L. Y. and Davis, G. W. (2014). Krüppel mediates the selective rebalancing of ion channel expression. *Neuron* **82**, 537-544.

Pédelacq, J.-D., Cabantous, S., Tran, T., Terwilliger, T. C. and Waldo, G. S. (2006). Engineering and characterization of a superfolder green fluorescent protein. *Nat. Biotechnol.* **24**, 79-88.

Pierce, S. B., Yost, C., Britton, J. S., Loo, L. W. M., Flynn, E. M., Edgar, B. A. and Eisenman, R. N. (2004). dMyc is required for larval growth and endoreplication in Drosophila. *Development* **131**, 2317-2327.

Pimentel, A. C. and Venkatesh, T. R. (2005). rap gene encodes Fizzy-related protein (Fzr) and regulates cell proliferation and pattern formation in the developing Drosophila eye-antennal disc. *Dev. Biol.* **285**, 436-446.

Sher, N., Von Stetina, J. R., Bell, G. W., Matsuura, S., Ravid, K. and Orr-Weaver, T. L. (2013). Fundamental differences in endoreplication in mammals and Drosophila revealed by analysis of endocycling and endomitotic cells. *Proc. Natl. Acad. Sci. U.S.A.* **110**, 9368-9373.

Sigrist, S. J. and Lehner, C. F. (1997). Drosophila fizzy-related down-regulates mitotic cyclins and is required for cell proliferation arrest and entry into endocycles. *Cell* **90**, 671-681.

Smith, A. V. and Orr-Weaver, T. L. (1991). The regulation of the cell cycle during Drosophila embryogenesis: the transition to polyteny. *Development* **112**, 997-1008.

Development (2014) 141, 2657-2668 doi:10.1242/dev.107573

Sugimura, K., Yamamoto, M., Niwa, R., Satoh, D., Goto, S., Taniguchi, M., Hayashi, S. and Uemura, T. (2003). Distinct developmental modes and lesion-induced reactions of dendrites of two classes of Drosophila sensory neurons. *J. Neurosci.* **23**, 3752-3760.

Tracey, W. D., Jr, Wilson, R. I., Laurent, G. and Benzer, S. (2003). painless, a Drosophila gene essential for nociception. *Cell* **113**, 261-273.

Truman, J. W. and Bate, M. (1988). Spatial and temporal patterns of neurogenesis in the central nervous system of Drosophila melanogaster. *Dev. Biol.* **125**, 145-157.

Truman, J. W. and Reiss, S. E. (1988). Hormonal regulation of the shape of identified motoneurons in the moth Manduca sexta. *J. Neurosci.* **8**, 765-775.

Tusher, V. G., Tibshirani, R. and Chu, G. (2001). Significance analysis of microarrays applied to the ionizing radiation response. *Proc. Natl. Acad. Sci. U.S.A.* **98**, 5116-5121.

Unhavaithaya, Y. and Orr-Weaver, T. L. (2012). Polyploidization of glia in neural development links tissue growth to blood-brain barrier integrity. *Genes Dev.* **26**, 31-36.

Weiss, A., Herzig, A., Jacobs, H. and Lehner, C. F. (1998). Continuous Cyclin E expression inhibits progression through endoreduplication cycles in Drosophila. *Curr. Biol.* **8**, 239-242.

Yamagishi, M., Ito, E. and Matsuo, R. (2011). DNA endoreplication in the brain neurons during body growth of an adult slug. *J. Neurosci.* **31**, 5596-5604.

Yasunaga, K.-i., Kanamori, T., Morikawa, R., Suzuki, E. and Emoto, K. (2010). Dendrite reshaping of adult Drosophila sensory neurons requires matrix metalloproteinase-mediated modification of the basement membranes. *Dev. Cell* **18**, 621-632.

Zielke, N., Querings, S., Rottig, C., Lehner, C. and Sprenger, F. (2008). The anaphase-promoting complex/cyclosome (APC/C) is required for rereplication control in endoreplication cycles. *Genes Dev.* **22**, 1690-1703.

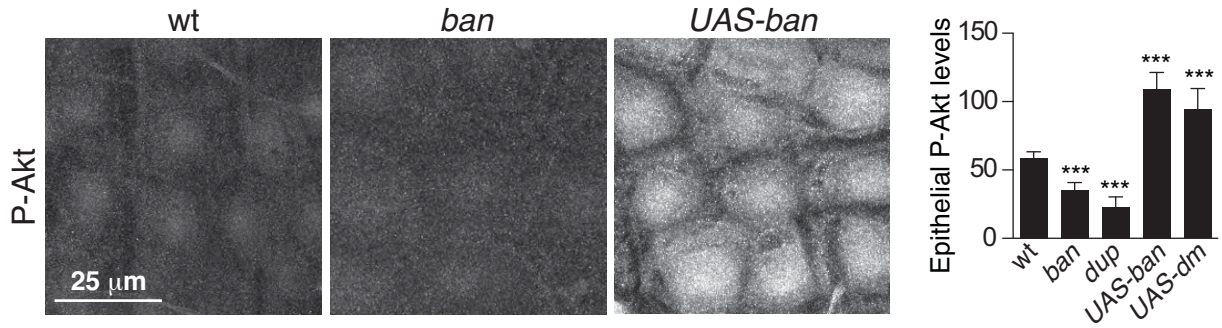

Figure S1. Phospho-Akt levels are responsive to *ban* activity and to endoreplication. Representative images of P-Akt staining in body wall epithelial cells of wild-type (wt), *ban* mutant, or epithelial *ban* overexpressing larvae are shown. Mean pixel intensity values for P-Akt staining. $n \geq 50$ cells for each genotype. Error bars represent standard deviation. ***$P<0.001$ compared to wt; one way ANOVA with a post-hoc Dunnett's test.

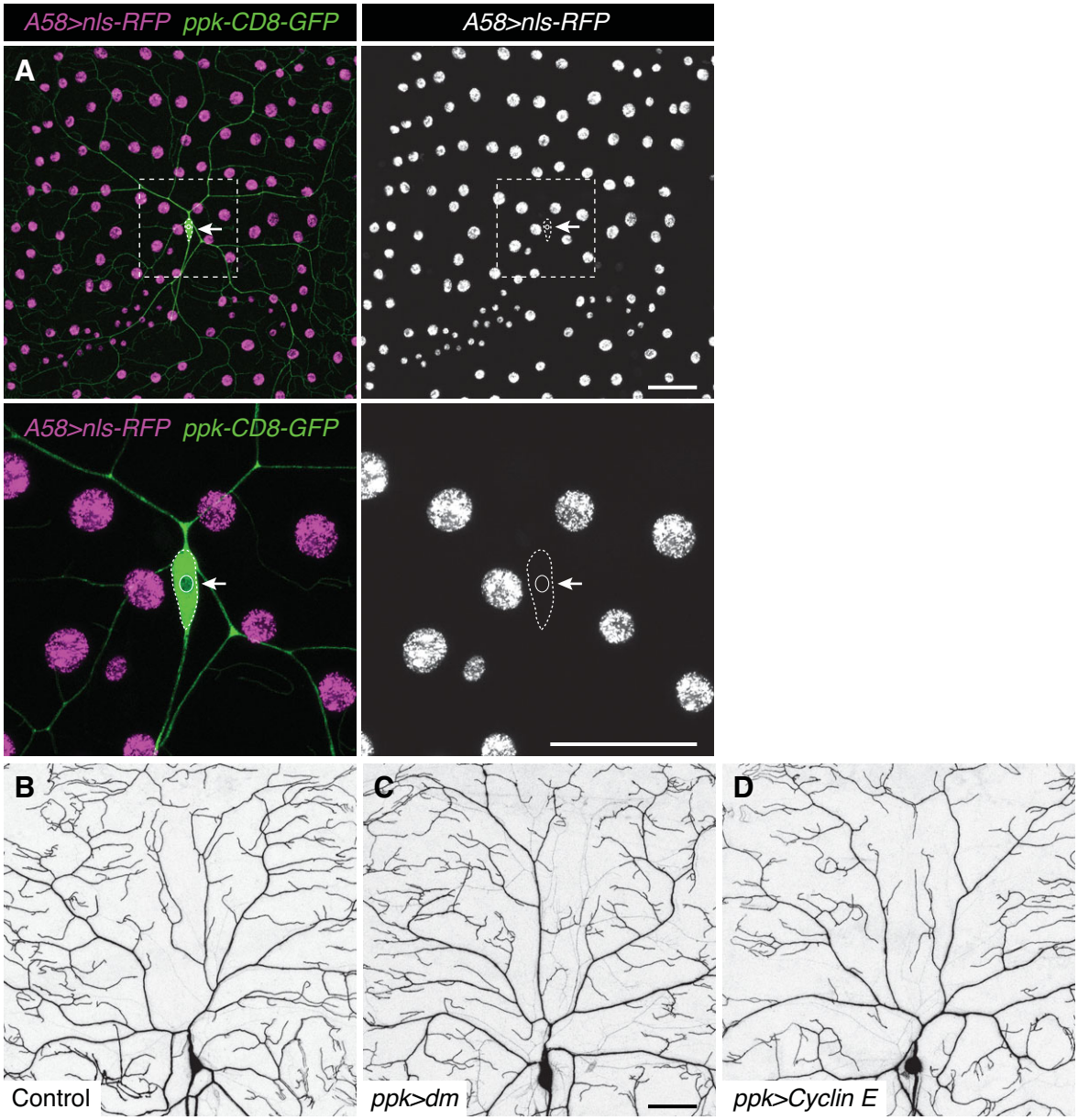

Figure S2. Epithelial specificity of *A58-Gal4* driver. (A) Larval *A58-Gal4* expression visualized by *UAS-nls-redStinger*. Although *A58-Gal4* is expressed throughout the epidermis, with the exception of apodemes, expression is not detectable in C4da neurons (arrow; labeled by *ppk-CD8-GFP*). (B-D) C4da dendrites in Control (*ppk-CD8-GFP, ppk-gal4* x w^{118}) larvae (B) or larvae overexpressing *UAS-dm* (C) or *UAS-Cyclin-E* in C4da neurons. Neuronal overexpression of endoreplication regulators does not alter C4da growth/patterning, demonstrating that dendrite growth defects caused by *A58*-driven expression of *UAS-dm* and *UAS-Cyclin-E* are not due to leaky neuronal expression of the driver. Scale bars, 50 μm.

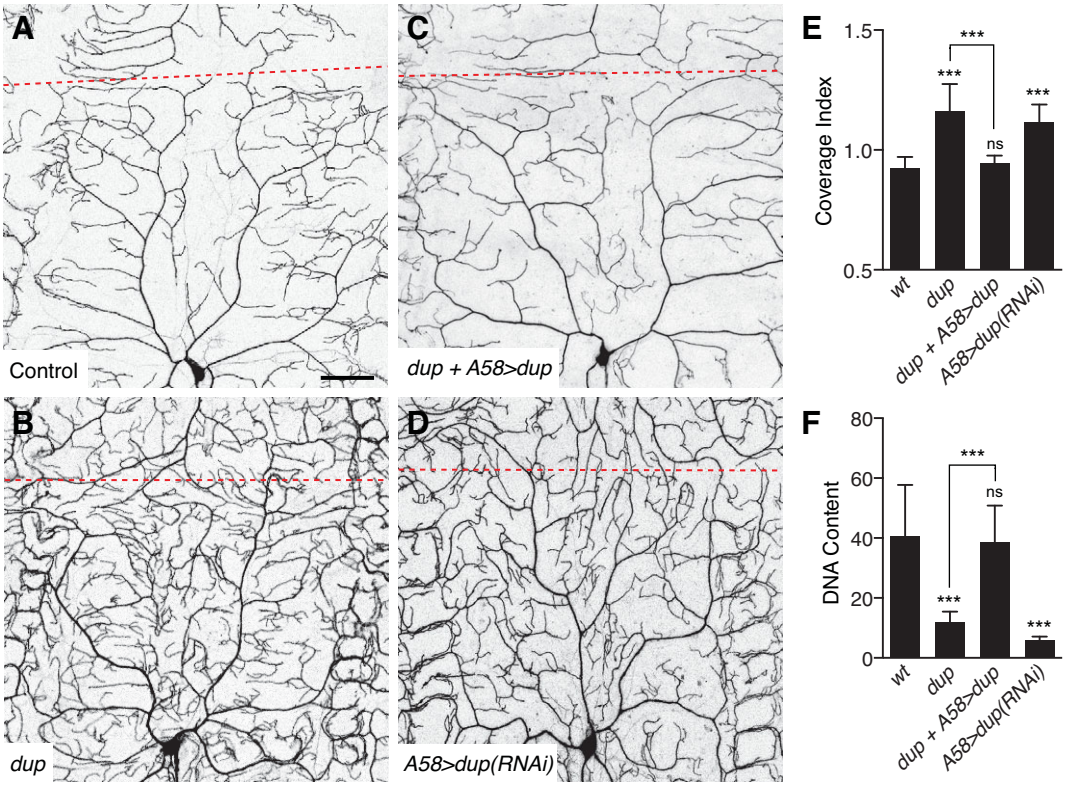

Figure S3. *dup* is required in epithelial cells to regulate epithelial ploidy and C4da dendrite growth. Compared to wt (A), blocking endoreplication with mutation in *dup* (B) increased dendrite growth and coverage. This dendrite overgrowth phenotype was completely rescued by resupplying *UAS-dup* to epithelial cells of homozygous dup mutant larvae (C). Epithelia-specific knockdown of *dup* (*A58>dupRNAi*) (D) caused dendrite defects comparable to dup mutation, demonstrating that dup is required in epithelial cells to support dendrite growth. (E) Quantification of dendrite coverage defects in the indicated genotypes. *n*=8 dendrites for each genotype. (F) *dup* is required in epithelial cells to support epithelial endoreplication. Quantification of DNA content in epithelial cells of the indicated genotype; measurements were as indicated in Fig. 2. *n*>20 cells for each genotype. Error bars represent standard deviation. **P*<0.05, ***P*<0.01, ***P*<0.001; ns, not significant; one-way ANOVA with a post-hoc Dunnett's test. Red dashed lines mark dorsal midline. Scale bars, 50 μm. Images in (A) and (B) are reproduced from Fig. 3.

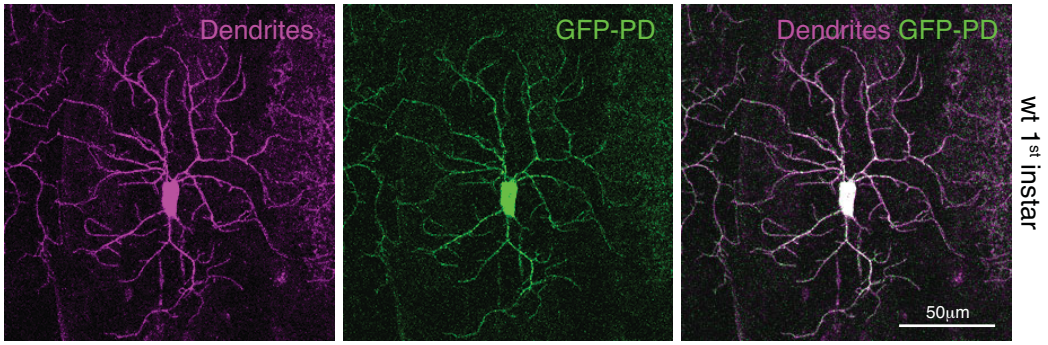

Figure S4. GFP-PD activity in first instar larvae.
Both halves of the proximity detector were expressed in C4da neurons (*ppk-gal4>UAS-sp1-10GFP* + *ppk-sp11GFP*) and GFP-PD activity was monitored in newly eclosed first instar larvae. Imaging settings were identical to those used in Figure 4.

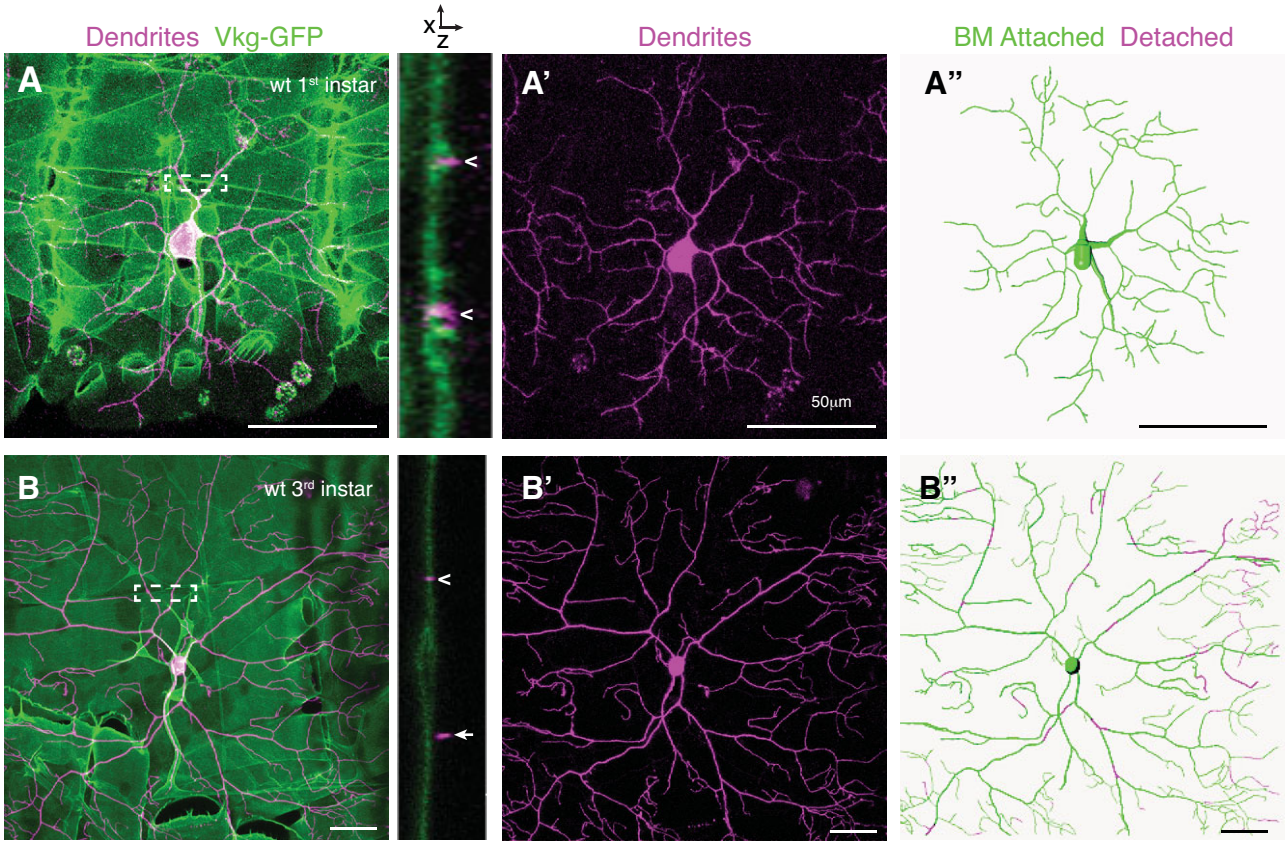

Figure S5. Live imaging of dendrites and the ECM using a neuronally-expressed membrane marker (*ppk-CD4-tdTomato*) and a GFP enhancer trap in *Drosophila viking* (*vkg-GFP*) to monitor dendrite-ECM colocalization. Representative maximum projections of 3D stacks captured by taking 200 nm optical sections are shown for wild type first instar larvae (A) and wild type third instar larvae (B). Orthogonal slices are shownfor the region marked by a white dashed box, and in the orthogonal slice attached dendrites are marked with carats (>) and detached dendrites are marked with asterisks (*). In the traces, dendrites that colocalize with Vkg-GFP are colored green whereas detached dendrites are colored magenta. Note the increase in dendrite detachment from the basement membrane in third instar larvae.

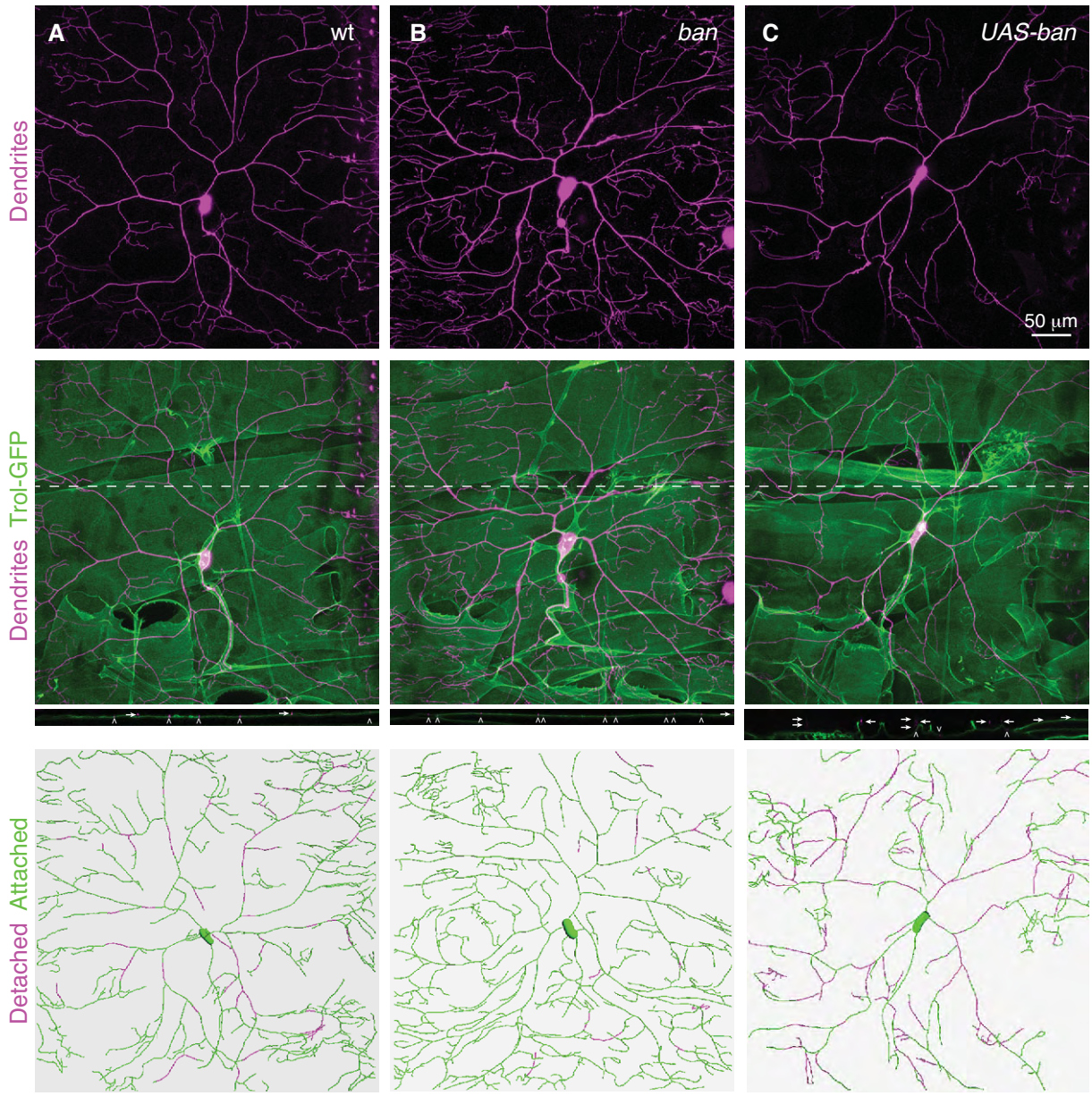

Figure S6. Live imaging of dendrites and the ECM using a neuronally-expressed membrane marker (*ppk-CD4-tdTomato*) and a GFP enhancer trap in the gene encoding *Drosophila* Perlecan (*trol-GFP*) to monitor dendrite-ECM colocalization in WT third instar larvae (A), *ban* mutant third instar larvae (B), and epithelial *ban* over-expressing instar larvae (C). 3D stacks were captured by taking 200 nm optical sections; maximum projections are shown. Following deconvolution, colocalization was measured between dendrites and Perlecan. Detached dendrites are marked with arrows in cross section and colored magenta in dendrite traces, whereas attached dendrites are marked with carets in cross section and colored green in dendrite traces.

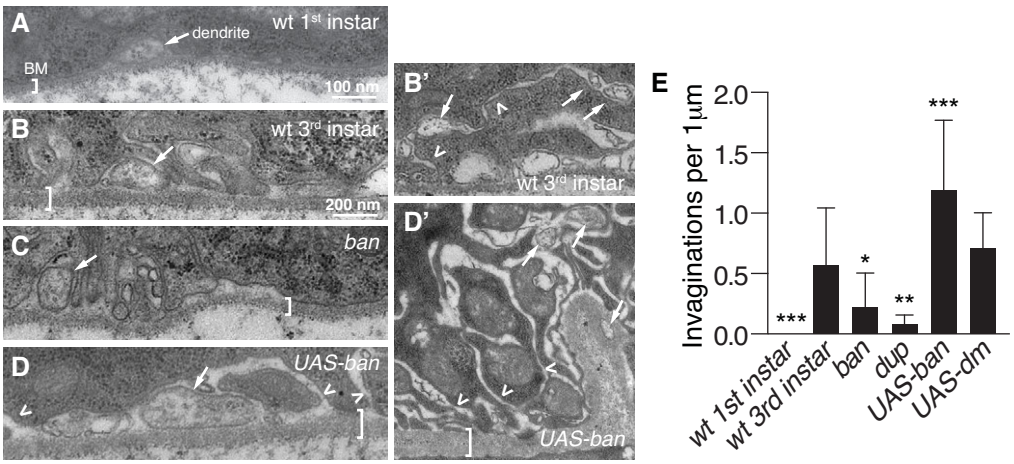

Figure S7. *ban* regulates epithelial internalization of dendrites. (A-D) TEM micrographs of the indicated genotypes. Dendrites (arrows) were identified as processes containing arrays of multiple parallel microtubules near the basal epithelial surface. Brackets mark BM; scale is identical in (B-D). (E) Epithelial basal plasma membrane invagination frequency was scored in 15 images (from multiple larvae) and the mean frequency of invaginations is plotted for the indicated genotypes. Other than wt first instar samples, all samples were from third instar larvae. Error bars represent standard deviation. **P*<0.05, ***P*<0.01, ****P*<0.001 compared to wt 3rd instar; one way ANOVA with a post-hoc Dunnett's test.

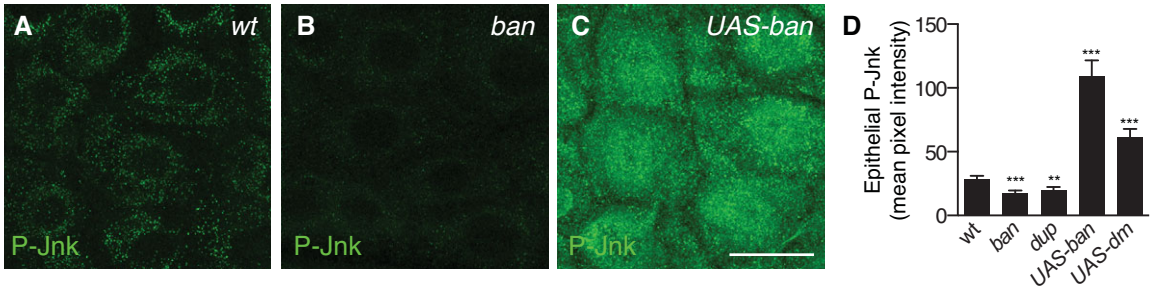

Figure S8. P-Jnk immunoreactivity in body wall epithelial cells is developmentally regulated by endoreplication. Representative images of P-Jnk staining in third instar body walls of wild-type (A), *ban* mutant (B), and epithelial *ban* overexpressing (C) larvae are shown. (D) Quantification of P-Jnk immunoreactivity for the indicated genotypes. Fillets of all genotypes were stained together with wild type fillets to ensure that staining conditions were comparable and all images were captured using identical settings. Means represent average pixel intensity of polygons outlining $n>50$ single cells (ImageJ). Error bars represent standard deviation. $^{**}P<0.01$, $^{***}P<0.001$; one way ANOVA compared to wild type with a post-hoc Dunnett's test. Scale bar, 25 μm.

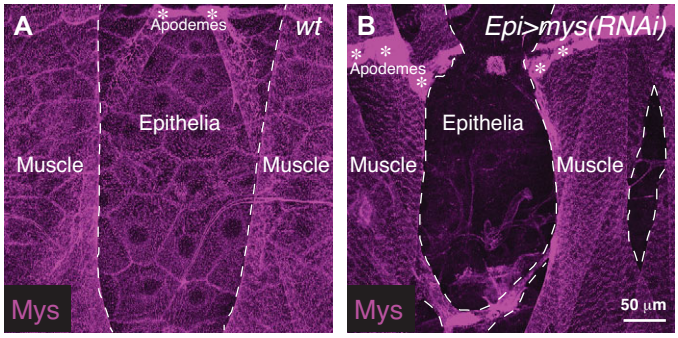

Figure S9. RNAi-mediated knockdown of epithelial Mys expression. Representative images of body wall Mys expression for wild type (A) and epithelial *mys(RNAi)* (B) are shown. Dashed white lines outline longitudinal muscles and asterisks mark apodemes. Note that epithelial *mys(RNAi)* effectively attenuates Mys levels in epithelial cells, but not muscle cells or apodemes, demonstrating the specificity of the Gal4 driver.

Table S1. ban-regulated transcripts in epithelial cells.

Up-regulated in 3rd instar *ban* mutant larvae

UNIQID	NAME	Fold Change	wild type (0013-b1)	wild type (0013-b2)	wild type (0013-b3)	wild type (0020-b1)	wild type (0020-b2)	ban (0020-b3)	ban (0020-b4)
ft01431	CG14957	54.38309826	-0.926	-0.386	-1.305	-1.655	-1.224	4.91	4.527
ft02983	mtrm	41.38135366	0.45	0	-0.518		0.018	4.87	5.697
fc31822	mTerf3	19.77716515	0.024	0	-0.198	-0.505	-0.831	3.817	4.231
fc31821	mTerf3	23.59403922	0.447	0.255	0.111	-1.784	-0.868	4.124	4.632
fc24392	Bem46	13.61779775	0.1655	0.0425	-0.2765	-0.2585	-1.2325	3.7425	3.2785
fc24391	Bem46	11.22019386	0.072	-0.127	-0.659	-0.122	-0.928	3.364	2.974
fc25516	CG8397	7.832427306	-0.8235	-0.7635	-0.7965	-0.4815	-0.6355	2.4775	2.0395
fc13695	CG14957	10.28335014	-0.805	-0.502	-0.958	0.192	0.038	3.276	2.725
ft09425	CG40002	13.98774469	-0.3715	-0.8865	-2.0935	-2.2515	-2.4645	2.2875	2.5775
fc00390	Pimet	13.43206545	0.5865	0.2905	-0.7045	-1.0885		3.3755	3.5795
fc29246	CG4570	9.002184093	-1.439	-1.888	-1.077		-1.374	1.854	2.051
ft08658	SC35	8.064435428	-0.304	0.228	-0.384	-0.534	-0.688	2.94	2.438
fc02453	grp	10.59343156	0.295	0.504	-1.001	-0.445	-1.148	3.173	3.222
fc24731	CG4594	10.68938941	0.554	0.419	0.326	-0.259	-0.875	2.972	3.946
ft05917	spn-E	10.22992091	0.4435	-0.2835	-0.1695	-0.0365	-0.7115	3.7355	2.5195
fc13376	CG4702	15.42497591	-0.357	0.511	-0.161	-0.018	-2.607	3.802	3.619
fc12616	PGRP-SA	13.40199442	-0.095	0.225	0.174	-1.422	-1.643	3.823	2.786
fc12617	PGRP-SA	14.21845636	0	0.296	0.207	-1.593	-1.786	3.933	2.906
fc31682	Ady43A	7.927964382	-0.548	-0.44	0.199	-0.784	-1.157	2.344	2.663
fc30581	Papst2	6.120105738	-0.958	-0.962	-1.334	-0.598	-1.18	1.692	1.563

Down-regulated in 3rd instar *ban* mutant larvae

UNIQID	NAME	Fold Change	wild type (0013-b1)	wild type (0013-b2)	wild type (0013-b3)	wild type (0020-b1)	wild type (0020-b2)	ban (0020-b3)	ban (0020-b4)
ft08217	Cyp4p2	0.012934911	4.111	3.925	4.629	4.643	5.013	-2.037	-1.52
ft05145	cad	0.016748094	2.6725	4.0835	2.6875	3.4785	4.0145	-2.0575	-2.8145
fc21832	CG4382	0.019567644	3.533	2.71	3.859	2.337	3.938	-1.954	-2.673
ft02746	CG14130	0.037092008	3.021	2.863	2.479	2.035	2.344	-2.942	-1.657
ft08080	CG12325	0.034088995	2.843	2.712	2.752	1.678	3.465	-1.83	-2.381
fc17436	Abl	0.066212955	1.009	1.393	1.546	1.719	1.097	-2.428	-2.66
fc03754	CG33667	0.032248651	-0.745	1.094	0.283	0.588	1.03	-4.145	-4.639
fr00526	snoRNA:Me28S-C788b	0.02076532	2.062	1.349	1.865	3.594	1.577	-4.846	-2.503
fc17435	Abl	0.062946773	0.819	1.318	1.381	1.607	0.848	-2.492	-3.095
fc21833	CG4382	0.013611545	4.582	3.77	5.095	1.825	4.022	-1.432	-2.967
fc26302	Sox102F	0.01082367	0.745	0.753	2.654	3.828		-3.251	-5.008
ft03571	CG4644	0.090373967	0.73	0.937	0.827	0.697	0.537	-2.442	-3.055
ft00305	rap	0.07176139	0.329	0.45	0.656	0.427	-0.186	-3.028	-4.018
ft07227	CG3409	0.078947074	-0.551	-0.173	0.019	-0.855	0	-3.571	-4.428
ft04329	CG8419	0.018947444	1.026	1.781	2.486	-0.745	-0.255	-4.424	-4.374
ft08088	CG30017	0.08883701	3.301	3.651	3.554	3.434	3	-0.997	0.466
ft02758	Grip163	0.042182724	1.9575	1.5485	1.4265	2.1055	3.6355	-4.0385	-1.3895
ft08218	Cyp4p1	0.012128943	2.518	1.866	0.923	2.887	-1.642	-4.187	-4.748
fc02315	CG3397	0.070869465	2.526	3.11	2.71	1.763	1.513	-1.176	-1.608
ft01633	CG15196	0.04496275	0.7745	1.6845	1.3925	2.4505	-0.1545	-3.6475	-2.5525
fc14739	Grip163	0.050937694	1.833	1.945	2.351	0.308	2.737	-1.917	-2.725
ft04133	Ucp4C	0.156783026	1.37	1.426	1.479	1.26	1.396	-1.13	-1.459
fc06063	hep	0.077451084	1.268	1.494	1.452	2.043	2.853	-1.999	-1.523
ft07069	CG31005	0.043455668	0.293	0.024	-0.442	2.152	1.047	-4.511	-3.046
fc06062	hep	0.093728032	1.621	1.803	1.861	2.404	2.896	-1.316	-1.126
ft09260	CG15400	0.10277636	-0.928	0.167	-0.086	-0.171	-0.186	-3.115	-3.972
ft05448	Crc	0.039040173	3.605	3.46	3.55	3.614	0.928	-2.454	-0.778
ft01119	CG30421	0.049349053	0.933	1.166	0	1.78		-3.507	-3.43
ft01748	sno	0.024643295	0.959	1.732	1.353		-2.074	-5.149	-4.029
fc03453	CG17568	0.048481514	-0.2445		-0.1635	1.0845	-0.0005	-4.1305	-4.5625
fc15527	Ir76a	0.027653221	2.7665	2.3435	3.9235	0.2465	1.1695	-2.0825	-3.3055
fc27070	CG9776	0.179058477	1.8765	1.9005	1.8515	1.8355	1.9335	-0.4625	-0.7555
fc20820	CG40244	0.010388539	-0.245	0.177	0.202	1.497	4.35	-4.062	-4.334
fc26243	slim	0.098689757	0.1835	-0.0245	1.0225	0.1945	1.1475	-2.3515	-3.3145
fc18150	sno	0.097995896	0.47	0.851	0.85		-0.242	-3.055	-2.853
ft03261	CG1529	0.035237435	1.7135	2.3955	2.7965	5.0575	2.7935	-0.5035	-3.6435
ft08475	CG31998	0.081798552	0.5825	1.7735	1.9395			-1.9975	-2.9125
ft02607	HGTX	0.027263781	1.67	3.241	1.161	-0.055	-0.431	-2.906	-4.4
fc01267	CG31469	0.014542143	0.503	0.13	0.145		4.186	-4.426	-3.475
fc20245	CG12065	0.114974181	0.337	1.099	0.864	0.208	0	-2.197	-3.043
fc03789	Tango6	0.070757702	1.771	2.01	2.479	3.337	3.339	-3.844	-0.199
ft06583	CG5794	0.111658002	2.114		2.865	2.429	2.151	-0.179	-1.985
ft04979	kel	0.15798186	0.7005	0.6715	0.9025	0.9405	1.2995	-1.8585	-1.6325
ft06594	CG13631	0.099913702	-0.487	-0.168	0.05	-0.05	1.076	-2.758	-3.635
fc32525	Cp7Fb	0.02045096	-0.034	0.6	1.659		4.197	-3.483	-2.947
fc02314	CG3397	0.068410779	2.353	2.903	2.57	1.765	0.56	-1.439	-1.881
ft08287	Cyp4e2	0.055960448	-0.719	-0.043	0.931	-0.362	1.852	-3.5	-3.509
fc27069	CG9776	0.176973115	1.59	1.639	1.558	1.885	1.873	-0.611	-0.977
fc10722	Obp57e	0.060088032		1.798	1.02		-0.898		-4.477
fc05719	Hsc70-2	0.021612465	2.27	2.771	3.261	4.677		-1.734	-3.158
fc16288	CG5794	0.143580054	2.429	2.441	2.926	2.709	2.448	0.278	-0.905
ft07164	CG17994	0.075834157	0.952	1.939	1.886	0.077		-1.452	-3.818
fc20244	CG12065	0.129118399	0.2815	0.9795	0.7035	-0.0275	0.0105	-2.2185	-2.8725
ft03054	RNaseX25	0.144217243	0.37	0.102	0.193	0.008	0.91	-2.696	-2.221
ft06749	scrib	0.108149673	3.768	4.256	4.214	4.325	4.581	-1.11	1.871
ft07931	Sin3A	0.095839888	0.34	-0.028	-0.326	1.272	1.15	-2.607	-2.941
ft00510	mys	0.091910806	1.529	1.355	2.007	0.49	0.312	-1.707	-2.848
fc05897	plexA	0.046323452	1.92	2.064	1.055	2.489	4.288	-1.355	-1.937
fc17672	tkv	0.135622406	1.352	1.716	1.122	1.876	1.518	-0.813	-2.184
ft03099	CG8596	0.095171726	0.723	0.713	1.99	2.243	1.793	-1.521	-2.058
fc03755	CG33667	0.061472178	-0.966	0.252	0.155	-1.629	1.034	-3.895	-4.051
fc31265	Imp	0.123685737	1.056	2.007	1.506	2.126	2.323	-0.825	-1.551
fc09500	S1P	0.08517687	0.793	0.688	1.277	1.474	2.708	-1.718	-2.253
fc32371	ssp3	0.168561006	1.025	1.241	1.094	1.359	0.906	-1.098	-1.875
fc28724	CG13875	0.083270432	1.4655	1.2545	1.3285	3.1805	2.0055	-3.0655	-0.8075

ft03236	slgA	0.088052903	0.665	0.838	0.607	2.482	1.573	-2.648	-1.669
ft08590	NijA	0.132144517	1.133	1.412	1.295	0.996	0.255	-2.449	-1.428
ft06577	CG6643	0.015425351	1.0485	0.5805	0.5215	0.3055	4.6665	-3.7015	-3.0795
ft00555	Corp	0.061488273	0.316	0.454	-2.335	0.154	-0.304	-3.648	-4.768
fc18151	sno	0.14575905	0.34	0.562	0.36	-0.34	0.361	-2.026	-3.183
fc16553	scrib	0.116822275	3.1	3.511	3.423	3.467	2.839	-2.645	1.088
ft07689	dup	0.128225639	-1.037	-0.415	-0.59	0.237	0.119	-2.849	-3.739
fc30028	ERR	0.080795735	0.228	0.116	0.589	2.091	1.811	-2.406	-2.443
fc13121	CG30438	0.175254878	0.6115	0.3955	0.7245	0.2485	0.0155	-1.8655	-2.3595
ft00803	CG4386	0.010980197	3.395	3.286	3.638	5.109	-1.415	-2.375	-3.263
fc03597	ppk6	0.083523396	1.805	2.543	1.854	0.307		-1.306	-3.013
ft05356	Mkk4	0.120219712	0.0025	0.4675	1.3625	0.6285	-0.0025	-1.8735	-3.5105
ft01398	Atg2	0.113662268	0.501	0.52	0.712	2.06	0.517	-2.162	-2.088
ft09402	eIF-4B	0.022793262	1.214	1.209	0.787	-2.554	2.646	-4.331	-3.902
fc23410	Cp1	0.086046054	0.726	0.942	1.143		2.851	-1.413	-2.877
fc05896	plexA	0.073567498	2.0955	2.2415	1.3015	2.4415	4.0575	-0.7325	-1.3755
ft06750	CG6490	0.116435078	0.7815	0.3775	1.0055	2.1325	1.3595	-2.3315	-1.4775
ft01163	gsb-n	0.024849994	2.443	2.113	4.316	0.474	-0.138	-2.829	-2.497
ft03114	Cpr65Ec	0.126890937	0.42	1.917	0.996	1.757	1.603	-1.461	-1.629
ft08342	CG30377	0.087536563	2.052	2.137	2.506	4.199	3.232	-0.522	-0.37
ft06004	Abd-B	0.060394391	0.492	1.667	0.042	2.587	2.708	-2.06	-2.331
ft05165	tadr	0.105343199	-0.103	-0.218	-0.229	-1.452	-1.668	-4.829	-3.253
fc12608	Sin3A	0.149982369	0.4035	0.6005	0.5685	0.6585	1.4055	-1.4455	-2.7785
ft03690	CG5585	0.13938445	1.533	1.527	0.815	0.456	0.594	-1.366	-2.375
fc21987	CG32043	0.133108973	1.594	1.787	2.328	2.884	2.139	-0.074	-1.789
ft06022	m-cup	0.117019094	-0.136	0.667	0.75	1.746	0.998	-1.607	-3.085
ft01052	enok	0.178197679	0.587	0.593	1.29	0.886	1.015	-1.267	-2.005
ft08752	CG33993	0.13001149	3.391	3.369	4.149	3.784	4.041	-2.462	1.764
fc32483	CG12340	0.154940793	0.036	-0.012	0.489	1.16	0.48	-2.014	-2.401
ft03749	CG7611	0.029581463	1.528	2.396	3.558		-1.221	-2.867	-2.907
fc04798	dream	0.205512178	-0.314	0.118	-0.122	0.181	0.14	-2.435	-2.122
fc29444	kuk	0.083183766	-0.1335	1.7765	2.3465	0.4105	1.4265	-1.9255	-2.4425
fc18444	CG32676	0.087946114	0.867	1.558		2.496	-0.153	-1.92	-2.192
fc20821	CG40244	0.019653282	-0.034	0.212	0.352	1.845	4.479	-2.772	-3.574
fc12416	topi	0.162256757	0.933	0.675	1.012	0.744	-0.103	-1.588	-2.359
ft04646	CG6792	0.074455263	0.271	-0.154	0.824	1.465	-1.507	-3.26	-3.269
fc03150	CG40337	0.08327479	1.064	1.406	2.099	3.251	0.713	-1.806	-1.372
fc11154	CG33272	0.025079144	1.779	2.327	2.683	0.104	5.156	-1.647	-2.334

Table S2. Genotypes used in this study.

	Panel	Label	X-chromosome	Chromosome II	Chromosome III
Figure 1	A	wt	w^{118}, *arm::GFP*^{wee}		
	A	*ban*	w^{118}, *arm::GFP*^{wee}		$ban^{\Delta}{}^{1}$/ $ban^{\Delta}{}^{1}$
	D	wt	w^{118}		
	D	*ban*	w^{118}		$ban^{\Delta}{}^{1}$/ $ban^{\Delta}{}^{1}$
	D	*UAS-ban*	w^{118}	*UAS-ban/+*	*A58-Gal4*
	E	wt	*hs-flp*^{122}	*Act-Frt-Stop-Frt-Gal4, UAS-tdTomato/+*	
Figure 2	A-I, J, K	wt	w^{118}		
	I-K	*ban*	w^{118}		$ban^{\Delta}{}^{1}$/ $ban^{\Delta}{}^{1}$
	J, K	*dup*	w^{118}	dup^{k03308}/dup^{k03308}	
	J, K	*rap*	w^{118}, rap^{G0418}		
	J, K	*UAS-ban*	w^{118}	*UAS-ban/+*	*A58-Gal4/+*
	J, K	*UAS-dm*	w^{118}	*UAS-dm/+*	*A58-Gal4/+*
Figure 3	A, G, H-J	wt	w^{118}, *ppk-3x-mCD8-GFP*		
	B, G	*ban*	w^{118}, *ppk-3x-mCD8-GFP*		
	C, G	*dup*	w^{118}, *ppk-3x-mCD8-GFP*		
	D, G	*UAS-CycE*	w^{118}, *ppk-3x-mCD8-GFP*	*UAS-CycE/+*	*A58-Gal4/+*
	E, G	*UAS-ban*	w^{118}, *ppk-3x-mCD8-GFP*	*UAS-ban/+*	*A58-Gal4/+*
	F, G	*UAS-dm*	w^{118}, *ppk-3x-mCD8-GFP*	*UAS-dm/+*	*A58-Gal4/+*
	G	*rap*	w^{118}, rap^{G0418}		*ppk-EGFP/ppk-EGFP*
	H	*ban/dup*	w^{118}, *ppk-3x-mCD8-GFP*	dup^{k03308}/+	$ban^{\Delta}{}^{1}$/+
	I	*dup +UAS-ban*		dup^{k03308}, *UAS-ban/* dup^{k03308}	*A58-Gal4, ppk-CD4-tdTomato/'ppk-CD4-tdTomato*
	J-K	*ban + UAS-dm*	w^{118}, *ppk-3x-mCD8-GFP*	*UAS-dm/+*	$ban^{\Delta}{}^{1}$, *A58-Gal4/* $ban^{\Delta}{}^{1}$
Figure 4	A, C, H, F, G	wt	w^{118}	*Ppk-CD4-tdTomato-T2A-sp11GFP/+*	*A58-Gal4/UAS-sp1-10GFP*
	D, F, G, I	*UAS-ban*	w^{118}	*Ppk-CD4-tdTomato-T2A-sp11GFP/UAS-ban*	*A58-Gal4/UAS-sp1-10GFP*
	E-G	*dup*	w^{118}	*Ppk-CD4-tdTomato-T2A-sp11GFP,* dup^{k03308}/dup^{k03308}	*A58-Gal4/UAS-sp1-10GFP*
Figure 5	A, B, G, H	wt	w^{118}	vkg^{G205}*(vkg::GFP)/+*	*ppk-CD4-tdTomato/ppk-CD4-tdTomato*
	C, G, H	*ban*	w^{118}	vkg^{G205}/+	$ban^{\Delta}1$, *ppk-CD4-tdTomato/*$ban^{\Delta}1$, *ppk-CD4-tdTomato*
	D, G, H	*UAS-ban*	w^{118}	vkg^{G205}/*UAS-ban*	*A58-Gal4, ppk-CD4-tdTomato/ppk-CD4-tdTomato*
	E, G, H	*dup*	w^{118}	vkg^{G205}, dup^{k03308}/ dup^{k03308}	*ppk-CD4-tdTomato/ppk-CD4-tdTomato*
	F-H	*UAS-dm*	w^{118}	vkg^{G205}/*UAS-dm*	*A58-Gal4, ppk-CD4-tdTomato/ppk-CD4-tdTomato*
Figure 6	A	wt	w^{118}, *arm::GFP*^{wee}		
	A	*ban*	w^{118}, *arm::GFP*^{wee}		$ban^{\Delta}{}^{1}$/ $ban^{\Delta}{}^{1}$
	B	wt	w^{118}		
	B	*ban*	w^{118}		$ban^{\Delta}{}^{1}$/ $ban^{\Delta}{}^{1}$
	B	*dup*	w^{118}	dup^{k03308}/dup^{k03308}	
	B	*rap*	w^{118}, rap^{G0418}		
	B	*UAS-CycE*	w^{118}	*UAS-CyclinE*	*A58-Gal4/+*

	B	*UAS-ban*	w^{1118}	*UAS-ban/+*	*A58-Gal4/+*
	B	*UAS-dm*	w^{1118}	*UAS-dm/+*	*A58-Gal4/+*
	C	wt	w^{1118}, *ppk-3x-mCD8-GFP*		
	D	*UAS-mysRNAi*	w^{1118}, *ppk-3x-mCD8-GFP*		*UAS-mysRNAi*^{HMS00043} */A58-Gal4*
	E	*UAS-ban + mysRNAi*	w^{1118}, *ppk-3x-mCD8-GFP*	*UAS-ban*	*UAS-mysRNAi*^{HMS00043} */A58-Gal4*
	F	*UAS-Integrins*	w^{1118}, *ppk-3x-mCD8-GFP*		*UAS-mys, UAS-mew*
	G	*ban + UAS-Integrins*	w^{1118}, *ppk-3x-mCD8-GFP*		*ban*^{s1}, *UAS-mys, UAS-mew/ A58-Gal4, ban*^{s1}
Figure 7	A-D	wt	w^{1118}	*ppk-CD4-tdTomato-T2A-sp11GFP/+*	*A58-Gal4/UAS-sp1-10GFP*
	E	wt	w^{1118}, *ppk-3x-mCD8-GFP*		
	F	*dup*	w^{1118}, *ppk-3x-mCD8-GFP*	*dup*^{k03308}*/dup*^{k03308}	
	G	*vkg*	w^{1118}, *ppk-3x-mCD8-GFP*	*vkg*^{01209}, *cn*^{1}*/ vkg*^{01209}, *cn*^{1}	
	H	*mysRNAi*	w^{1118}, *ppk-3x-mCD8-GFP*		*UAS-mysRNAi*^{HMS00043} */A58-Gal4*
Figure S1		wt	w^{1118}		
		ban	w^{1118}		*ban*^{s1}*/ ban*^{s1}
		UAS-ban	w^{1118}	*UAS-ban/+*	*A58-Gal4/+*
Figure S2		wt	w^{1118}	*ppk-CD4-tdTomato-T2A-sp11GFP/+*	*ppk-Gal4/UAS-sp1-10GFP*
Figure S3	A	wt	w^{1118}, *trol*^{zcl1700} *(trol::GFP)*		*ppk-CD4-tdTomato/ppk-CD4-tdTomato*
	B	*ban*	w^{1118}, *trol*^{zcl1700}		*ban*^{s}*1, ppk-CD4-tdTomato/ban*^{s}*1, ppk-CD4-tdTomato*
	C	*UAS-ban*	w^{1118}, *trol*^{zcl1700}	*UAS-ban/+*	*A58-Gal4, ppk-CD4-tdTomato/ppk-CD4-tdTomato*
	D	*UAS-dm*	w^{1118}	*UAS-dm/+*	*A58-Gal4/+*
Figure S4		wt	w^{1118}	*vkg*^{G205}*(vkg::GFP)/+*	*ppk-CD4-tdTomato/ppk-CD4-tdTomato*
Figure S5	A	wt	w^{1118}		
	B	*ban*	w^{1118}		*ban*^{s1}*/ ban*^{s1}
	C	*UAS-ban*	w^{1118}	*UAS-ban/+*	*A58-Gal4/+*
	E	*dup*	w^{1118}	*dup*^{k03308}*/dup*^{k03308}	
	E	*UAS-dm*	w^{1118}	*UAS-dm/+*	*A58-Gal4/+*
Figure S6	A	wt	w^{1118}		
	B	*ban*	w^{1118}		*ban*^{s1}*/ ban*^{s1}
	C	*UAS-ban*	w^{1118}	*UAS-ban/+*	*A58-Gal4/+*
	D	*UAS-dm*	w^{1118}	*UAS-dm/+*	*A58-Gal4/+*
Figure S7	E	wt	w^{1118}, *ppk-3x-mCD8-GFP*		
	F	*UAS-mysRNAi*	w^{1118}, *ppk-3x-mCD8-GFP*		*UAS-mysRNAi*^{HMS00043} */A58-Gal4*

Supplemental Materials and Methods

Dendrite measurements

To measure dendrite coverage, we used three indices. The coverage index represents the portion of the larval body wall covered by dendrites of a single neuron in dorsal hemisegments bounded by muscle attachment sites (apodemes; anterior/posterior boundaries), the dorsal midline (dorsal boundary) and a line connecting a neuron of interest to the corresponding neuron in the adjacent segments (ventral boundary). A dendrite that completely covers the dorsal hemisegment would have a coverage index of 1 whereas a dendrite that covered the entire dorsal hemisegment and territory of neighboring hemisegments would have a coverage index of > 1. The Invasion Index represents the portion of a dorsal hemisegment that is covered by dendrites of neurons from neighboring hemisegments. Midline occupancy represents the dendrite density at the midline and is expressed as dendrite length/unit area (μm dendrite length/1000μm^2).

Fluorescence-activated cell sorting (FACS)

Larvae were filleted in PBS and the tissue containing cells of interest was dissected away from all other tissues. Dissection time was limited to 30min per sample, and following dissection cell suspensions were prepared in 5 volumes of PBS/2x trypsin via 3 cycles of the following: triturate 10x through a 1000 microliter pipet tip, mix 5min at 1000 rpm in a 37°C microtube mixer. Cell suspensions were filtered through a 70um cell strainer and sorted on a FACSAria II (BD). GFP^+ non-autofluorescent events were sorted into RNAqueous-Micro Lysis buffer (Life Tech.) and frozen on dry ice.

RNA isolation, amplification, and microarray hybridization

RNA was isolated from FACS-sorted samples using an RNAqueous-Micro kit (Life Tech.) and DNase-treated. All RNA samples were subjected to two rounds of linear amplification using the Aminoallyl MessageAmp II kit (Life Tech.). Dye-coupled aRNA was fragmented and hybridized to custom-designed microarrays (Agilent).

Microarray design

We hybridized our samples to custom-designed 4x44k feature oligonucleotide microarrays (Agilent, Santa Clara, CA). We designed two 60-mer oligonucleotide probes for each of the 20,726 coding sequences in the annotated fly genome (release 5.2) using ArrayOligoSelector (Bozdech et al., 2003), resulting in 35,272 successful probe designs, 16,717 additional probes against alternatively spliced transcripts, and 546 probes targeting non-coding RNA (244 snoRNA, 108 tRNA, 24 snRNA, 74 rRNA, 3 miRNA, 93 other). The final probe set was filtered to remove redundant probes, overlapping probes, and those with cross hybridization potential (based on a -21.6 kcal/mol threshold, which was chosen to fit the number of probes allowed in the Agilent 4 x 44k design specification). This resulted in 33,792 probes to CDS, 8744 probes to alternatively spliced transcripts, and 546 RNA probes. In total, 43,803 probes were included in the design.

Microarray scanning, feature extraction, normalization, and filtering

Microarrays were scanned on an Axon 4000B scanner and feature information extracted in GenePix 6 (Molecular Devices). GPR files were uploaded into Acuity (Molecular Devices) and ratio normalized. Data was retrieved using quality filters for reference

channel intensity, background intensity, pixel saturation, pixel variance, feature diameter, % pixel intensity over background, and feature circularity. “Ratio of Medians” data was further filtered for 70% present data, Cy5 net median intensity > 350 across a minimum of 3 arrays, Cy3 net median intensity > 150 across a minimum of 20 arrays. Expression ratios were $\log_2$ transformed, arrays median centered, quantile normalized, and genes median centered before analysis.

References

Bozdech, Z., Zhu, J., Joachimiak, M. P., Cohen, F. E., Pulliam, B. and DeRisi, J. L. (2003). Expression profiling of the schizont and trophozoite stages of Plasmodium falciparum with a long-oligonucleotide microarray. *Genome Biol.* **4**, R9.